

Dual Functional Styrene-Maleic Acid Copolymer Beads: Toxic Metals Adsorbent and Hydrogen Storage

R.B. Amal Raj, Renuka R. Gonte, and K. Balasubramanian

Abstract When the concentration of heavy toxic metals exceeds the constraint, adverse health effects in human as well as in other living organisms materialize. Even though the entire evading of exposure to such metals is not possible, abstraction of such metals is effected by either physical or chemical processes such as adsorption, electrochemical methods, chemical precipitation, ultrafiltration and coagulation floatation. Precipitation or oxidation-reduction methods which convert the metal ions to insoluble compounds or extortionate sludges during the metal ion isolation may lead to a secondary pollution. Of these methods, adsorption is accepted as one of the most adequate and fiscal methods for the abstraction of metal ions at low ion concentrations. This chapter spotlights on the cross-linked styrene-maleic acid copolymeric beads for the adsorption of toxic heftily ponderous metal ions from aqueous systems and a material for hydrogen storage at room temperature. The suspension polymerized adsorbents were highly cross-linked to achieve better mechanical properties, and the porosity is introduced in the copolymer matrix. Discrete metal ions such as Cu(II), Co(II), Ni(II), Zn(II) and Au(III) and dyes such as Congo red (CR) were magnificently adsorbed by the highly cross-linked styrene-maleic acid copolymeric beads. XRD and SAXS results verified that these copolymer beads are additionally highly efficacious in in situ reduction of Au (III) ions from dihydrogen monoxide to Au (0) nanogold formation. The obtained experimental data were interpreted utilizing distinct adsorption isotherms and kinetic models such as Freundlich isotherm, Langmuir isotherm, Temkin isotherm, pseudo-first-order kinetic model, pseudo-second-order kinetic model and intraparticle diffusion models. Langmuir and Freundlich isotherm models were fitting for the adsorption of metal ions and are followed by pseudo-first-order kinetics in the initial stages and pseudo-second-order kinetics in the later stage of adsorption. Adsorption of metal ions was governed by intraparticle diffusion, and the desorption of metal ions was carried out utilizing dilute HCl. To assess the

R.B. Amal Raj

Centre for Biopolymer Science and Technology, A Unit of CIPET, Cochin 683501, India

R.R. Gonte • K. Balasubramanian (✉)

Department of Materials Engineering, Defence Institute of Advanced Technology (DU),
Ministry of Defence, Pune 411 025, India

e-mail: meetkbs@gmail.com

adsorption of Congo red dye molecules, composites of SMA with sugarcane molasses and sawdust were additionally synthesized, and the composite exhibits exceptional adsorption of Congo red dye which was validated utilizing distinct isotherm and kinetic models. The adsorption of hydrogen by the cross-linked SMA copolymer beads at room temperature withal was evaluated. The augmented rate of hydrogen adsorption was prosperously accomplished by the prelude of highly cross-linked interpenetrating networks inside the microspheres and porosity prelude into the copolymer network. The rate of hydrogen adsorption is virtually commensurable for the various cross-linked polymers and is independent of their divinylbenzene content. Even with perpetuated exposure of upto 65 hours, saturation cannot be accomplished; thus the slow micropore opening mechanism being involved that is more immensely colossal pores are filled first is envisaged. Enhanced cross-linked SMA beads modified with metal-organic frameworks (MOF) were synthesized by the slow diffusion of TEA. Maleic acid, which is a dicarboxylic acid, will influence the morphology of the MOFs composed in the polymer matrix and thus the hydrogen storage capacity. SMA functionalized with MOF samples exhibit hydrogen storage capacities where Zn-SMA complexes exhibit hydrogen storage capacity of 0.57 wt% at 300 K and 0.61bars. The ethanol adsorption and retention of the modified beads can be scrutinized for a cache of liquid hydrogen in fuel cells. Advantages in the utilization of these polymer beads in fuel cell encompass embedded catalyst activity, low cost, efficacious solvent and simultaneous hydrogen storage and operation at higher temperatures, thus providing a solution for current fuel cells.

Keywords Metal pollution • Styrene-maleic acid copolymer beads • Adsorbent • Hydrogen storage

Introduction

Recent years have experienced incrementing cognizance for water pollution, and its far-reaching effects have prompted concerted efforts towards pollution abatement (Donmez et al. 1999). Rapid industrialization has solemnly contributed to the relinquishment of toxic heftily ponderous metals in the water streams. Many industrial wastewaters contain substances that are difficult to abstract via conventional secondary treatment; are toxic or hazardous; are volatile and cannot be transferred to the atmosphere; have the potential for engendering noxious vapours or odours, or for imparting colour to the wastewater; and are present in diminutively minuscule concentrations that make their abstraction via other methods difficult. Mining, electroplating, metal processing, textile and battery manufacturing industries are the main sources of heavy metal contamination (Babel and Opiso 2007; Nwuche and Ugoji 2008). These activities pollute dihydrogen monoxide streams, especially rivers, and make them lose their potential value and benign use (Celik and Demirbas 2005; Kadirvelu et al. 2001). Contamination of aqueous

environments by heftily ponderous metals and dyes is a worldwide environmental concern due to their toxic effects and accumulation through aliment chain (Kapoor et al. 1999; Sternberg and Dorn 2002). Amongst these heavy metal ions, the ions of Cd, Zn, Hg, Pb, Cr, Cu, As, etc., have gained consequentiality due to their highly toxic nature even at low concentrations. The high concentration of these heavy metals in the environment can be detrimental to a variety of living species. Extortionate ingestion of these metal ions by humans can cause accumulative poisoning, cancer, nervous system damage and ultimately death (Corapcioglu and Huang 1987; Issabayeva et al. 2007). Abstraction of trace amounts of heavy metal ions from wastewater and imbibing dihydrogen monoxide is of great paramountcy on account of their high toxicity (Gundogan et al. 2004; Abdel-Ghani et al. 2009; Resmi et al. 2010).

Adsorption finds applications in tertiary waste water treatment as a polishing step before final discharge into nearby. Adsorption is commonly used in the treatment of industrial wastewaters containing organic compounds not easily biodegraded during secondary (biological) treatment or toxic (Al-Rekabi et al. 2007). Adsorption using ion-exchange resins is one of the most popular methods for the removal of heavy metals from the water and wastewater (Omer et al. 2003; Rengaraj et al. 2004). Ion-exchange resins have been developed as a major option for treating wastewaters over the past few decades (Rawat et al. 1990; Rengaraj et al. 2007). Porous materials such as clay (Jaber et al. 2005), activated carbon (Zhu et al. 2009), zeolites (Wingenfelder et al. 2009) and biomass (Deng and Ting 2005) are usually used as toxic metal ion adsorbents because of their high surface area, large pore volume and the presence of exchangeable ions presenting themselves as good candidates for adsorbents. For better adsorption performance, the pore size of a porous adsorbent should match the adsorbates atomic/molecular size (Yang 2003).

Hydrogen is considered as a potential alternative for fossil fuel due to its attractive properties such as nontoxicity, clean combustion and high energy density (Schlapbach and Zuttel 2001). The chemical energy of hydrogen is approximately three times larger than the energy density of liquid hydrocarbon (Schlapbach 2002). Hydrogen storage will be required particularly for vehicular applications, stationary power generation, hydrogen delivery and refueling infrastructure. However, a number of significant technological hurdles need to be overcome for realizing these applications including safe, compact and high-capacity hydrogen storage systems. Physisorptive hydrogen storage on porous materials is considered to be potential method for vehicular application with a view of storage of large amounts of hydrogen at near-ambient temperatures and safe pressures. Porous polymers, such as hypercross-linked polymers, integrate incipient merits to the adsorbent family because of their low cost, facile processing and high thermal and chemical stability (Davankov and Tsyurupa 1990; Lee et al. 2006).

Sorbents may be synthetic or natural which include activated carbons (Rivera-Utrilla et al. 2003); zeolites (Inglezakis et al. 2003); clays (Yavuz et al. 2003; Al-Ashah et al. 2003); silica beads (Krysztafkiewicz et al. 2002); low-cost adsorbents such as industrial by-products (Netpradit et al. 2004; Gupta and Suhas 2009), agricultural wastes (Robinson and Chandran 2002) and biomass (Vasudevan et al.

2003); and polymeric materials like organic polymeric resins (Zhang et al. 2003; Atia et al. 2003) and macroporous hypercross-linked polymers (Azanova and Hradil 1999; Pan et al. 2003) to name as few as significant examples. Polymeric adsorbents possess rigid microporous structure with large surface area (greater than 1000 m²/g) (Goltz et al. 1994). Commercially available resins in bead form (typically 0.5 mm diameter) are usually composed of copolymers of styrene-divinylbenzene (DVB) and acrylic acid ester-divinylbenzene which possess a wide range of surface porosities, polarities and macropore sizes. The porosities can be built through emulsion polymerization, and this creates a polymer matrix with surface areas ranging up to 1100 m²/g (Thomas and Crittenden 1998; Yang 2003). Another advantage possessed is the inclusion of functional groups in the polymer matrix enhancing its adsorptive capacity. Styrene-divinylbenzene, polymethacrylate, divinylbenzene-ethylvinylbenzene, vinylpyridine, sulphonated or chloromethylated ion-exchange resins are a few examples of widely used adsorbents (Har et al. 2001; Toro et al. 2009). Polymeric adsorbents are possible by controlling/tailoring their pore structure and on-site regenerability (Leng 2009). In fact, the polymeric sorbents used for cyclic adsorption processes should satisfy the following requirements: large selectivity derived from equilibrium, kinetic or steric effect, large adsorption capacity, fast adsorption kinetics, easy regenerability, improved mechanical strength and low cost (Den 2006). Tailoring the adsorbent properties to meet the above requisites can result in adsorbents with immensely colossal internal pore volume, internal surface area, controlled surface properties through culled functional groups, controlled pore size distribution and impuissant interactions between adsorbate and adsorbent.

In this chapter we have successfully developed well-organized styrene-maleic acid copolymer beads and composites for adsorption of toxic chemicals and hydrogen as a highly innovative and eco-friendly method that can be employed for large-scale cleanups of water and as a storage material for hydrogen. Chemical modification of the SMA beads was also carried out by a simple transformation technique characterized by different techniques. The synthesis of polymeric adsorbents in the form of spherical beads is carried out using three different types of heterogeneous polymerization technique, viz., suspension polymerization, precipitation polymerization and emulsion polymerization (Oadian 2004). Special techniques such as FTIR spectroscopy, UV-visible spectroscopy, scanning electron microscopy (SEM), X-ray diffraction technique (XRD), small-angle X-ray scattering (SAXS) and thermogravimetric analysis (TGA) have been developed in order to characterize and study the properties associated with the materials.

In fact, adsorption isotherms are important to describe the adsorption mechanism for the interaction of metal ions/dyes on the adsorbent surface, for the design of an adsorption process, and to determine the efficiency of adsorption. Several adsorption isotherms pristinely utilized for gas phase adsorption are available and rarely adopted to correlate adsorption equilibria in heavy metal/dye adsorption. Some well-known ones are Freundlich, Langmuir, Temkin and Dubinin-Radushkevich (D-R) (Febrianto et al. 2009). To investigate the mechanism of adsorption and its potential rate-controlling steps that include mass convey and chemical reaction processes, kinetic models have been exploited to analyze the experimental data.

Several kinetic models such as pseudo-first-order, pseudo-second-order, Elovich and intraparticle diffusion have been applied to examine the rate-controlling mechanism of the adsorption process. Thermodynamic considerations are paramount to conclude whether the adsorption process is spontaneous or not. The adsorption of metal ions/dye onto adsorbents is studied at fine-tuned temperature.

Experiment and Characterization

Cross-Linked SMA Beads

Synthesis of Cross-Linked SMA Beads

Styrene (S) and divinylbenzene (DVB) were purified by extracting with 10% sodium hydroxide to remove the monomethyl hydroquinone (MEHQ) inhibitor and washed repeatedly with distilled water till pH of the elute was 7 (Fig. 1a) and finally dried over anhydrous calcium hydride. Maleic anhydride (MAN) and azobisisobutyronitrile (AIBN) were recrystallized from 80:20 chloroform/methanol mixture prior to use (Deb and Mathew 1996). Homogeneous solution of the purified monomers (styrene, maleic anhydride), cross-linker (DVB) and initiator (AIBN) was obtained in methyl isobutylketone (MIBK) under nitrogen atmosphere (Fig. 1b). A four-neck reaction vessel equipped with an overhead stirrer, purging tube, thermometer vial and water condenser was placed in oil bath. The organic

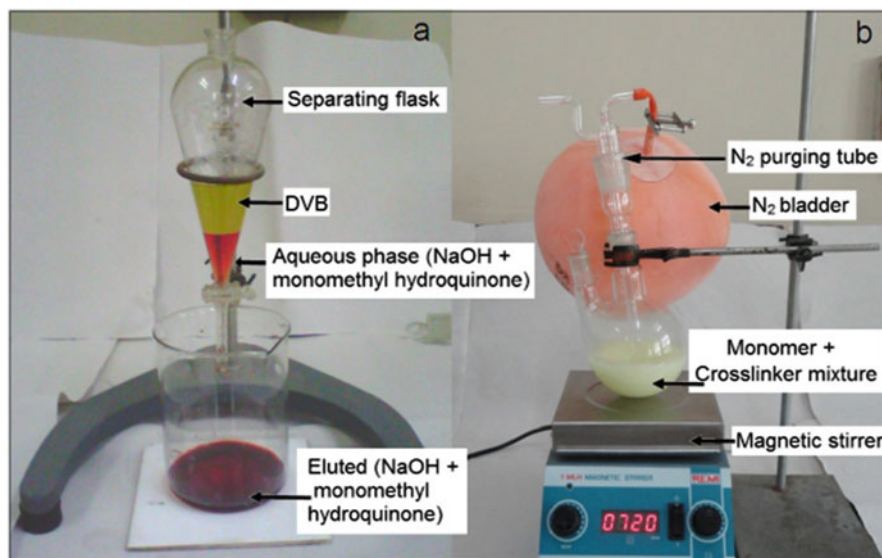


Fig. 1 (a) Purification of DVB; (b) monomer-cross-linker mixture (Gonte 2013)

monomer solution was added to this reaction vessel containing aqueous solution saturated with sodium chloride and in situ formed magnesium hydroxide from the reaction between magnesium chloride and sodium hydroxide, under continuous agitation at 60 °C (Deb and Mathew 1996). The water-to-monomer ratio was kept to 4:1 during polymerization. The monomer droplets converting to polymer particles were prevented from coalescing by continuous agitation and optimized $\text{Mg}(\text{OH})_2$ formation (suspension stabilizers).

Characterization

The density and cross-linking density of the synthesized cross-linked SMA beads were determined. The conversion of maleic anhydride to maleic acid and the functional group analysis of the copolymer were carried out using FTIR (Shimadzu Model FTIR-8400). JEOL ASM 6360A scanning electron microscope (SEM) was used to study the structural morphology. Thermogravimetric analysis was carried out using a thermal analyzer (Shimadzu Model TGA-50) to determine the thermal stability of the copolymer beads. Swelling capacity of the SMA beads was determined in ethanol.

Cross-Linked SMA as Adsorbent

Preparation of Metal Ion and Dye Solution

Single metal ion stock solutions (2000 mgL^{-1}) were prepared dissolving the copper sulphate pentahydrate ($\text{CuSO}_4 \cdot 5\text{H}_2\text{O}$), cobalt chloride ($\text{CoCl}_2 \cdot 6\text{H}_2\text{O}$), nickel sulphate ($\text{NiSO}_4 \cdot 6\text{H}_2\text{O}$), zinc sulphate ($\text{ZnSO}_4 \cdot 7\text{H}_2\text{O}$) and chloroauric acid ($\text{HAuCl}_4 \cdot 3\text{H}_2\text{O}$) salts in 1000 mL water. Stock solution of Congo red dye and direct red dye was prepared with concentration of 100 mgL^{-1} in water. The various experimental concentrations were then obtained by diluting the stock solution.

Batch Adsorption Experiments

The adsorption of Zn(II) ions was carried out by using 0.5 g beads soaked in 30 mL ZnSO_4 solution of various concentrations (200 mgL^{-1} , 250 mgL^{-1} and 500 mgL^{-1}) for 2 h, and at the end of the desired set time duration, 1.0 mL of supernatant solution was used to detect the concentration of the metal ions remaining in the solution. The effect of solution pH on adsorption was observed for a batch of 0.5 g SMA in 30 mL solution of concentration 100 mgL^{-1} . The amount of SMA beads was also varied from 0.2 to 1.0 g for fixed metal ion concentration (250 mgL^{-1}) for 2 h to obtain another set of data. The concentration of the metal ions was evaluated

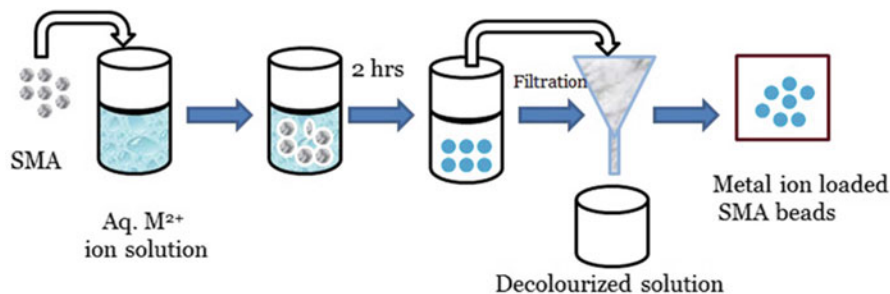


Fig. 2 Schematic presentation of batch adsorption process (Gonte 2013)

by titrating fixed volume of Zn(II) solution at specific time interval against standard EDTA solution (Gonte et al. 2011a, b). For Cu(II), Co(II), Ni(II), Au(III) ions, Congo red and direct red dye, adsorption was determined spectrophotometrically at 720 nm, 510 nm, 660 nm, 310 nm, 500 nm and 500 nm, respectively. The schematic presentation of the batch adsorption study is as shown in Fig. 2.

SMA Biocomposites

Synthesis of SMA-Sawdust (SMA-SD) Composites

The composite of styrene-maleic acid sawdust (SMA-SD) was synthesized by suspension polymerization as described in copolymer synthesis. Sawdust was washed in distilled dihydrogen monoxide to abstract any adhering impurities, dried and sieved. The homogeneous coalescence of organic monomers, i.e. styrene, MAn, DVB and free radical initiator AIBN (0.8 wt% predicated on monomers), was yare in MIBK solvent. The aqueous phase consisting of saturated salt solution (NaCl , $\text{Mg}(\text{OH})_2$) was yare in reaction vessel. The two phases were commixed together under inert conditions. When the gel point of the polymerization was achieved at about 70 °C, fine sawdust (by wt%) was integrated to the polymerization cumulation and stirred at 800 rpm to obtain the composite beads of 300–600 μm . These SMA-SD composite beads were then isolated from the aqueous phase and washed perpetually with dihydrogen monoxide, followed by toluene, to abstract unreacted monomers and with dilute hydrochloric acid for abstraction of magnesium hydroxide and determinately dihydrogen monoxide washed to abstract the acid and salts adhering to the surface of the polymer beads (Shelar et al. 2011).

Synthesis of SMA-Sugarcane (SMA-SM) Composites

Sugarcane molasses were obtained and washed repeatedly with distilled water, dried and sieved. The composites of styrene-maleic acid-sugarcane molasses (SMA-SM) were synthesized by the above mentioned process.

Batch Adsorption of Metal Ions and Dyes

Spectroscopic detection and quantification method as described in batch adsorption experiments was used for batch adsorption process for removal of dye (Congo red dye) and inorganic pollutants (Cu(II), Ni(II) and Co(II) ions) from aqueous solution. 100 mgL⁻¹ concentrations of the dye were prepared as the stock solution, while the stock metal ion solution was of concentration 1000 mgL⁻¹. Cu(II), Co(II), Ni(II) and Congo red dye were determined spectrophotometrically at 720 nm, 510 nm, 660 nm and 500 nm, respectively.

Chemically Modified SMA Beads

Synthesis of SMA Metal-Organic Frameworks

SMA-metal-organic frameworks were synthesized by a slight modification of the literature method of slow diffusion of TEA (Li et al. 1998). Briefly, dimethylformamide (DMF) solution containing Zn(NO₃)₂·6H₂O and dicarboxylic acid in a ratio of 1:2 mole % was diluted using toluene. The requisite amount of SMA beads was allowed to swell in this solution. The mixture was placed under reduced pressure for 5 h to ensure complete filling up of pores of SMA beads. After 5 h, the supernatant liquid was decanted, and slow vapour diffusion of triethylamine (TEA) in toluene was allowed. The system was sealed and kept undisturbed for 2 days at room temperature 300 K. SMA beads were then washed with DMF and dried under vacuum at 50 °C to constant weight. Three different dicarboxylic acid linkers, namely, 1,4-benzenedicarboxylic acid (BDC), 1,6-naphthalenedicarboxylic acid (NDC) and 1,8-biphenyldicarboxylic acid (BPDC), were used in the formation of MOFs with Zn(II) as the central metal ion. The schematic formation of Zn-SMA-DCA frameworks is shown in Fig. 3.

In another method of formation of SMA-MOFs, no additional dicarboxylic acid was used. Instead the Zn(II) ions were allowed to react with the carboxylic acid groups of SMA to form Zn(II) SMA complexes or Zn-SMA metal-organic frameworks (Deb et al. 2005; Gonte et al. 2011a, b). The schematic presentation is shown in Fig. 4.

Synthesis of SMA Polyaniline Semi-interpenetrating Networks

The synthesis of SMA-PANI semi-interpenetrating networks was based on a literature report by P C Deb (Deb et al. 2005). Benzoyl peroxide was recrystallized from 1:1 chloroform/methanol solution. Aniline was vacuum distilled prior to use. The semi-IPNs were synthesized by oxidative polymerization of aniline with benzoyl peroxide. The oxidative polymerization of aniline to polyaniline (PANI)

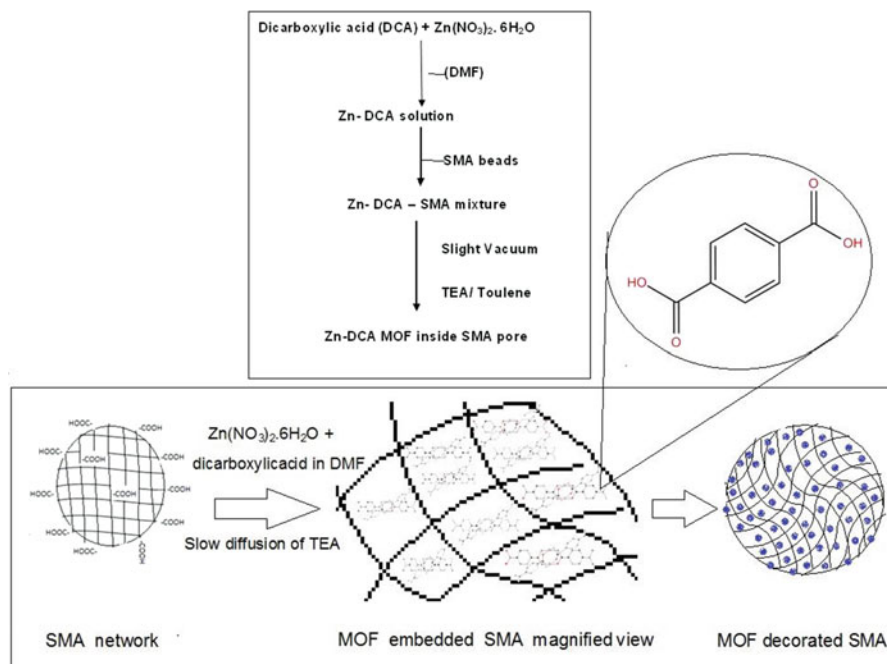


Fig. 3 Schematic representation of formation of Zn-SMA-DCA MOFs (Gonte 2013)

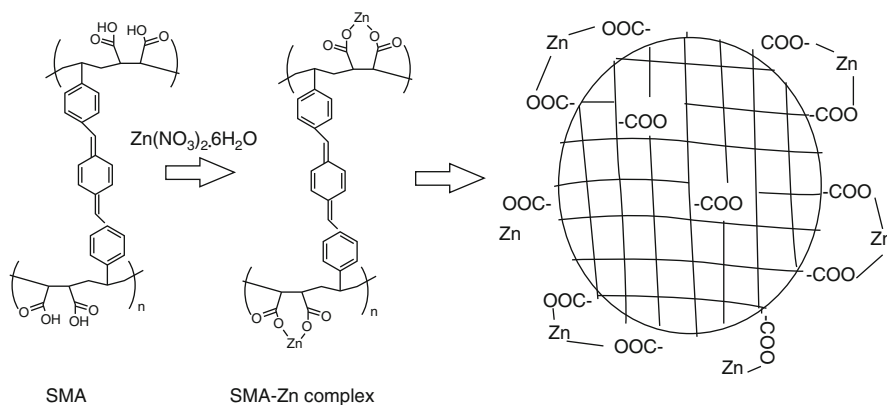


Fig. 4 Schematic representation of formation of Zn-SMA-MOFs (Gonte 2013)

is known to form emeraldine type of polyaniline. The schematic representation of which is shown in Fig. 5.

Known weight of SMA microspheres was suspended in acetone solution containing 0.6 M benzoyl peroxide and evacuated to remove entrapped air as well as to allow easy entry of BP solution inside the pores of SMA beads.

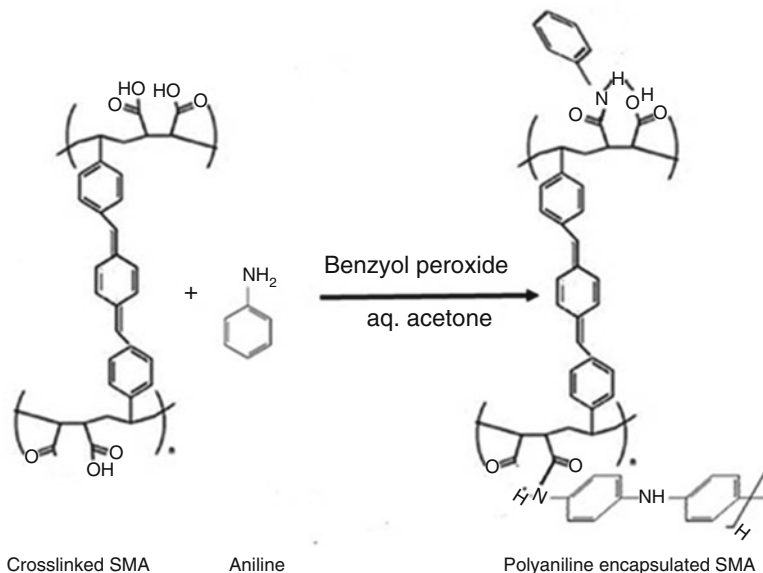


Fig. 5 Schematic representation of formation of SMA-PANI semi-IPNs (Gonte 2013)

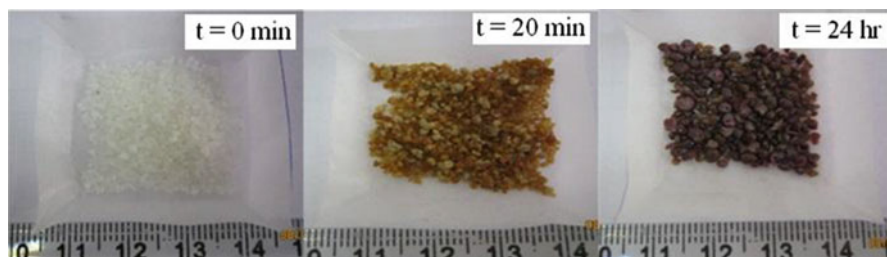


Fig. 6 Colour displayed by SMA beads during formation of SMA-PANI semi-IPNs (Gonte 2013)

The copolymer beads were then repeatedly washed with acetone to remove excess of BP. These microspheres were then added to aqueous acetone solution of freshly distilled aniline, and the mixture was stirred slowly but continuously for 24 h. The colour of the SMA beads changed from pale yellow to brown black in 15 min on stirring indicating the start of polymerization of aniline. The colour of the beads was further changed to purple black indicating polyaniline formation after 24 h as shown in Fig. 6. The solution containing fine black particles was decanted off, and the copolymer was purified by continuous soxhlation using acetone and then dried at 50 °C under reduced pressure to constant weight (Gonte et al. 2011a, b).

Characterization of Chemically Modified SMA Copolymer Beads

The modified SMA beads were characterized using Fourier transform infrared (FTIR) spectroscopy, scanning electron microscopy (SEM), thermogravimetric analysis (TGA) and swelling capacity in ethanol.

Hydrogen Adsorption

Hydrogen gas adsorption studies were carried out using SORPTOMATIC 1990 instrument (Thermo Finnigan, Italy), which records the fall of pressure and automatically converts the same into amount of gas adsorbed as per ASTM standards. The instrument was standardized with hydrogen and nitrogen to determine the dead volume. About 0.7 g of beads was evacuated (10–6 torr) at 343 K for 2 h in a previously evacuated glass sample holder to ensure cleanliness of surface and availability of clean pores for adsorption. A typical measurement for sample was continued for about 24 h at room temperature 300 K.

Result and Discussion

Cross-Linked SMA Beads

Effect of Experimental Parameters

Under the optimized reaction conditions, five different compositions of the cross-linked SMA beads were synthesized by varying the cross-linker content in the reaction mixture which is summarized in Table 1. The yield for all the compositions was found to be almost constant ($\approx 70\%$). The size of the cross-linked copolymer beads was found to be highly influenced by the stirring speed of the overhead stirrer. The effect of rpm on the bead diameter was investigated by carrying out the speed of the overhead stirrer to 400 rpm, 600 rpm and 800 rpm. The organic phases, when stirred with the aqueous phase under varying agitation speed, dispersed the monomers in the form of minute droplets along with the aqueous phase. The size of the droplet formed thus controls the bead diameter. During polymerization process, the viscosity of the medium also increases, and at the gel point, beads start to gain

Table 1 Synthesis data for SMA copolymer beads

Polymer designation	A1	A2	A3	A4	A5
S:MA (mole ratio)	1:1.6	1:1.6	1:1.6	1:1.6	1:1.6
S:DVA (mole ratio)	1:0.26	1:0.41	1:0.53	1:0.66	1:0.80

Table 2 Effect of agitation speed on the bead size

rpm	400	600	800
Bead dia (μ)	800–1000	300–500	200–400

Table 3 Calculated parameters of the SMA copolymer beads

Copolymer	Density (ρ) (g/mL)	Pore volume (V_p) (mL)	Porosity (Φ)	Crosslink density ($\times 10^{-3}$)
A1	0.892	1.878	1.565	8.980
A2	0.909	2.176	1.813	9.543
A3	0.919	1.918	1.598	11.546
A4	0.933	1.715	1.429	11.748
A5	0.951	1.645	1.370	11.344

shape. The control of rpm at and after this stage of polymerization is particularly important. It was observed that, with stirring speed of 200 rpm, there was a tendency of the beads to adhere post-polymerization, resulting in formation of a hard mass. The bead diameter as a function of controlled rpm control is presented in Table 2.

True Density, Pore Volume, Porosity and Cross-Link Density

True Density

Cross-linked SMA copolymer beads (1.0 g) were dried to constant weight (W_o) and placed in a 10 mL specific gravity bottle of known weight at 27 °C. Ethanol (7.0 mL) was added to this bottle, and the mixture was maintained under identical conditions for 24 h at 27 °C. The specific gravity bottle was then filled with ethanol and weighed carefully (Wan et al. 2004). The true density of the cross-linked SMA beads was calculated and is summarized in Table 3.

$$\rho = \frac{W_o}{10 - \frac{W_1 - W_o}{d_s}}$$

where W_1 is the total weight of beads and solvent and d_s is the density of solvent ($d_s = 0.789$ g/mL).

Pore Volume and Porosity

Known amount of SMA beads were placed in a sintered glass tube, and the entire assembly was placed in ethanol at 27 °C for 24 h. The excess solvent was removed and volume of ethanol absorbed by the beads was estimated V_p was estimation; porosity (Φ) of the beads was calculated following methods of Rosenberg et al. (1983), Greig and Sherrington (2003) and Wan et al. (2004) as follows:

$$V_p = \frac{W_o}{\rho}$$

$$\phi = \frac{V_p}{V_o}$$

where V_p is the pore volume in the beads, V_o is the true volume of the beads, W_o is the weight of dry beads and ρ is the true density of the polymer.

Cross-Link Density

The cross-linking density ρ_c of the cross-linked SMA beads was calculated from the Flory-Rehner equation (Wan et al. 2004):

$$\rho_c = \frac{1}{(2M_c)^{-1}}$$

where M_c is the average molecular weight per cross-linking unit calculated as

$$M_c = \frac{\left[\rho \times V_s \times \left(V_r^{\frac{1}{2}} \frac{V_g}{2} \right) \right]}{- \left[\ln(1 - V_r) + V_r + \chi V_r^2 \right]}$$

where V_r is the volume of polymer in the swollen state equilibrium, χ is the polymer solvent interaction parameter taken as 0.5, V_s is the molar volume of solvent and ρ is the true density of the polymer.

CHNS-Elemental Analysis

The CHN analysis of the cross-linked beads was performed in CHNS analyzer, Elementar Vario 111. The elemental analysis of total carbon and hydrogen provides the composition of the polymeric matter. It could be clearly seen from the obtained data (Table 4) that the carbon content of the copolymer beads increases with increase in the cross-linker (DVB) concentration of copolymer compositions. The carboxyl content of the polymer is reduced due to introduction of high density of

Table 4 Elemental composition of the copolymer beads

Copolymer	%C	%H	%O
A1	80.26	7.709	12.031
A2	83.11	8.033	8.857
A3	83.56	8.102	8.857
A4	81.35	7.531	11.119
A5	85.56	8.042	6.398

cross-linking. The elemental analysis data indicates the presence of 1.879, 1.383, 1.302, 1.737 and 0.999 millimoles of maleic acid per gram of polymer A1, A2, A3, A4 and A5, respectively. However, sudden increase in carboxyl content was observed with A4 beads. This may be due to pronounced association of cross-linker and maleic anhydride leading to higher content of acid in the copolymer. Increasing the DVB content increases the cross-linking intensity and porosity of the networks (Gonte et al. 2012).

FTIR Spectroscopic Analysis

The FTIR spectra of the cross-linked SMA beads were recorded on Shimadzu spectrophotometer to confirm the presence of carboxylic acid and styrene functional groups in the synthesized polymer (Fig. 7).

The FTIR spectra show the presence of peaks around 2930 and 2840 cm^{-1} corresponding to the asymmetric and symmetric stretch of C-H_2 , while the peak positioned at 2930 cm^{-1} corresponds to the OH stretch of carboxylic acid. The presence of 3500 cm^{-1} and 1710 cm^{-1} (shoulder peak) confirmed the free acid formed after hydrolysis of anhydride groups of cross-linked copolymer, and the broad band peak around 3000 cm^{-1} indicates the presence of high concentration of COOH groups. Bands at 3000 cm^{-1} , 2920 cm^{-1} and 2850 cm^{-1} correspond to the asymmetric and symmetric C-H stretch, and the peaks around 1943–1728 cm^{-1}

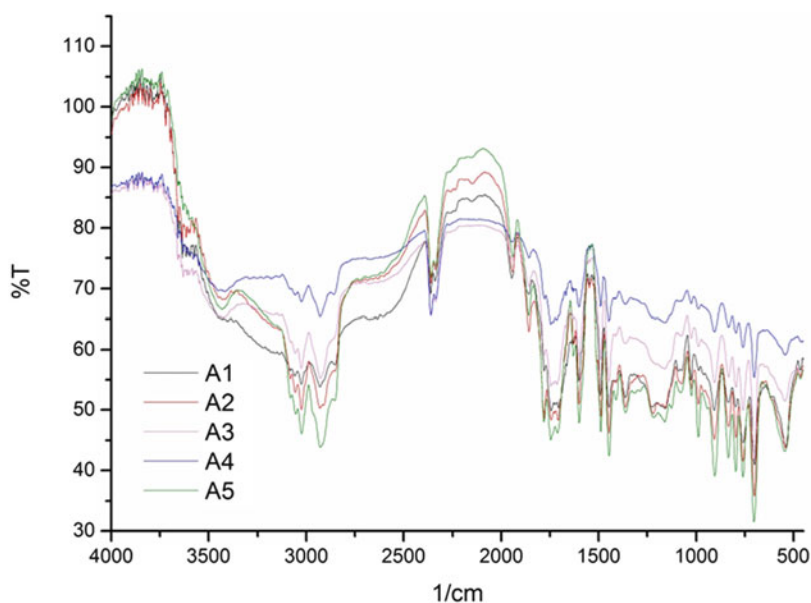


Fig. 7 IR spectra of cross-linked copolymer beads (Gonte 2013)

correspond to the aromatic ring substitution of styrene groups. The peaks within range $3100\text{--}3000\text{ cm}^{-1}$ correspond to aromatic stretching vibrations. Peaks at 1461 cm^{-1} and 1561 cm^{-1} represent $\text{C}=\text{C}$ (stretch) of the aromatic ring and carboxylate ion peak, respectively. Absorption peak at 3020 cm^{-1} characterizes $=\text{C}\text{--}\text{H}$ stretching for aromatic fragments. Thus the presence of both maleic acid and styrene groups in the copolymer beads was confirmed from the IR spectra for all the 05 compositions of cross-linked SMA beads.

SEM Analysis

The SEM analysis of the copolymer beads was performed to analyze the variation occurred by increasing the cross-linker content in the beads. The SEM images of the copolymer beads were obtained by coating the beads with an ultrathin coating of electrically conducting material (platinum) either by low-vacuum sputter coating or by high-vacuum evaporation. These coated samples were then mounted on the SEM moulds and scanned. The low-magnification SEM images confirmed the spherical shape of the beads, while the magnified micrographs revealed the presence of fissures, flow lines, micropores and voids. Increase in the microporosity and development of well-defined flow lines were observed with increase in the DVB content in the polymer beads as can be seen from Fig. 8.

The SEM images also indicate the increased compact packing observed in the beads with increasing divinylbenzene content suggesting the establishment of rigid interpenetrating network formation and increased cross-linking. Homogeneity in the pore size is also observed with increase in cross-linking, and thereby distinct fineness is introduced in the internal structure (Gonte et al. 2012). The SEM micrographs were then analyzed using the Biovis Material Plus software to estimate the pore size and pore density. The micrographs show uniform distribution of pores in size up to $75\text{ }\mu\text{m}$.

Thermogravimetric Analysis

The thermogravimetric analysis showed that the cross-linked copolymer is thermally stable up to $400\text{ }^{\circ}\text{C}$ (Gonte et al. 2011a, b), and complete decomposition occurs after $450\text{ }^{\circ}\text{C}$ as can be observed from Fig. 9. The initial slight notch observed at around $220\text{ }^{\circ}\text{C}$ is due to the decomposition of maleic acid to maleic anhydride which remains as the residue after even complete combustion of the copolymer and is reflected as residual weight. The shape decrease in the temperature around $400\text{ }^{\circ}\text{C}$ corresponds to the decomposition of styrene groups of the copolymer. The nature of curve with the various compositions of the SMA beads follows a similar pattern indicating that the increased DVB content shows no significant effect on the thermal stability of the copolymer.

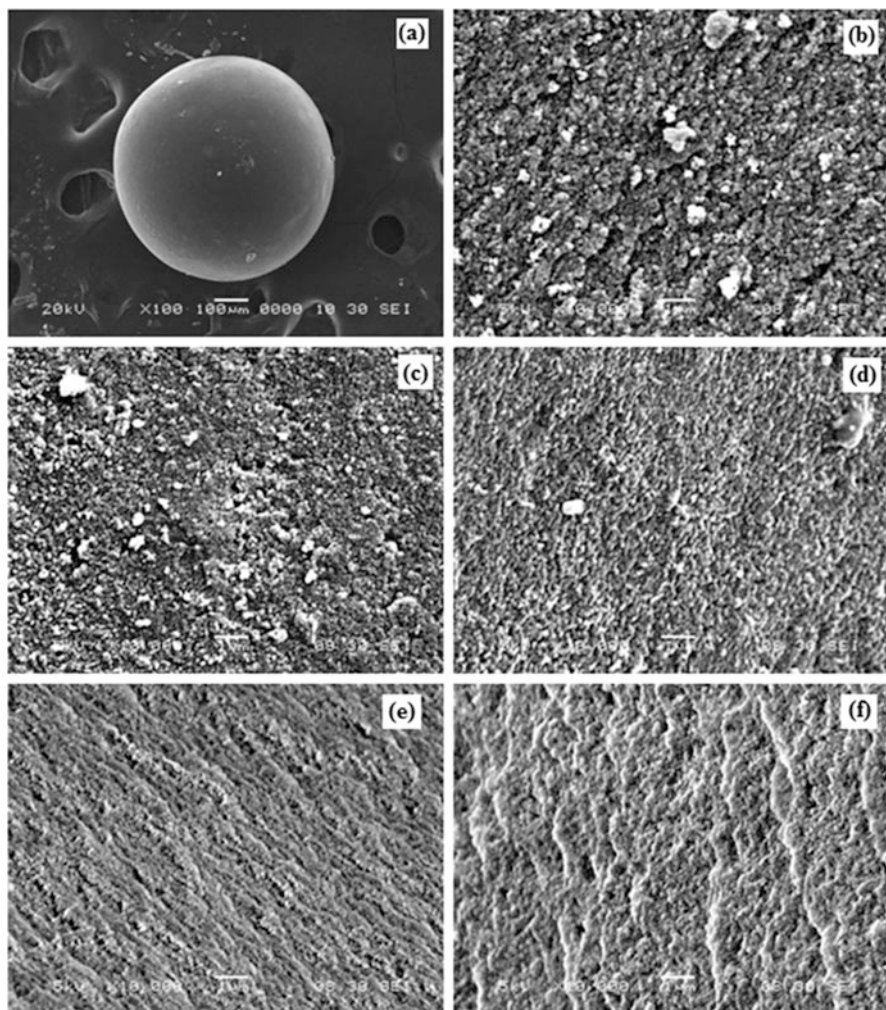


Fig. 8 SEM micrograph of the samples; (a) low-magnification SEM image of SMA; high magnification micrographs of (b) A1, (c), A2 (d), A3 (e), A4 and (f) A5 (Gonte 2013)

Cross-Linked SMA as Adsorbent

Characterization of the Metal Ion-Loaded SMA Copolymer Beads

The SEM images of the metal ion-adsorbed SMA beads showed no significant change in the morphology of the beads. The presence of the metal ion in the adsorbents was observed around the fissures and voids on the external surface of the beads. The presence of the metal ions in the beads was confirmed from the EDX analysis. The FTIR spectra indicated the slight decrease in the intensity of the

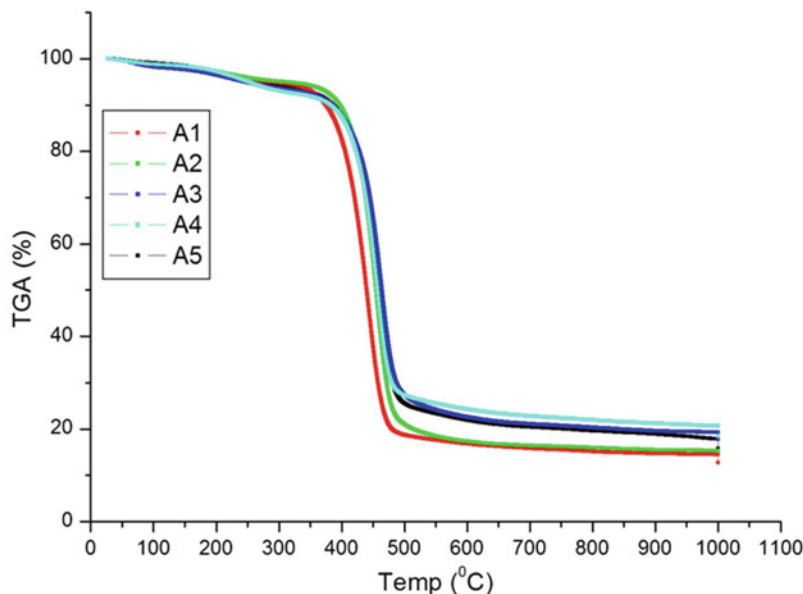


Fig. 9 Thermogravimetric curves of SMA beads (Gonte 2013)

carboxylate ion 1710 cm^{-1} peak noted after adsorption and complex formation between the metal ions and carboxyl group of the beads. The formation of varying colours of the beads on adsorption of Au(III) ions indicated the formation of nanogold within the polymer matrix which was confirmed from the XRD analysis. The XRD pattern for the Au(III) ion-embedded polymer matrix revealed the peaks with d spacing of 2.3427, 1.4388 and 1.2612. The appearance of these diffraction peaks in the gold ion-adsorbed SMA bead, indicates the presence of pure gold in nano form embedded into the polymer matrix (Gonte et al. 2011a, b). This reduction of Au(III) to Au(0) was observed due to the presence of trace amount of sodium ions entrapped in the polymer matrix during synthesis as an impurity. The XRD analysis of the metal ion-adsorbed beads is shown in Fig. 10. The XRD analysis of the metal ion-adsorbed beads shows the peak corresponding to d spacing of 4.04, 2.66, 2.47 and 1.96 for Cu(II) complexes; d spacing of 8.57, 5.57, 5.03 and 3.36 for Co(II) complexes and d spacing of 2.64, 2.188 and 1.16 for Ni(II) complexes with SMA beads (Sicilia-Zafrac et al. 1999; Deshdmukh and Deshpande 2011). Additionally, the core sizes of the embedded nanogold were deduced from the SAXS data. The small-angle X-ray scattering confirmed the presence of spherical agglomerates with typical radius of 48 nm and presence of larger aggregates of size in the range of 200 nm.

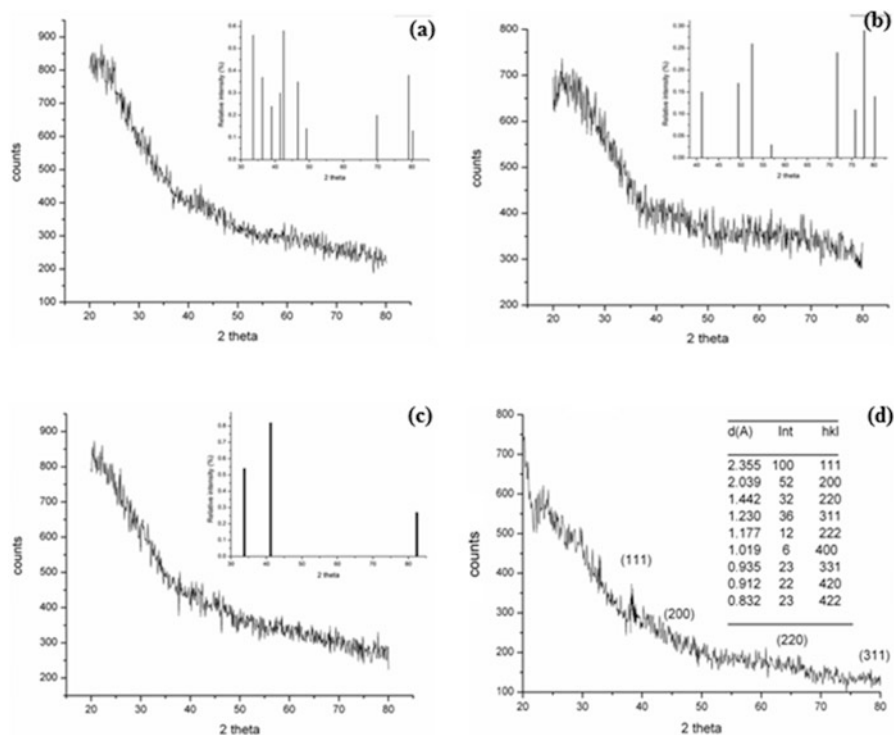


Fig. 10 XRD spectrum of SMA complexes with (a) Cu(II), (b) Co(II), (c) Ni(II) and (d) Au(III) (Gonte 2013)

Effect of pH

The removal of metal ions from aqueous solutions by adsorption was found to be highly dependent on the pH of the solution. Adsorption of Cu(II), Co(II), Zn(II) and Ni(II) ions was observed for increases with an increase in the pH from 4.0 to 8.0 as shown in Fig. 11. The decrease in the adsorption below pH 6 can be explained by the fact that at pH below 6.0, the H_3O^+ ions present in the aqueous solutions compete with the free metal ions for the active sites with carboxylic groups. The carboxyl groups get protonated which block the site for adsorption, and further the steric hindrance created by the protonation of acid decreases the metal ion uptake. The increase in the adsorption efficiency of the SMA with increase in pH from 4.0 to 7.0 was observed in case of all four metal ions, which suggests that the mechanism of uptake is same in all cases. In the case of Congo red and direct red dye, adsorption was attempted at its neutral pH 7.0 since both these dyes were found to be chemically and structurally stable at this pH. Drastic colour change was noticed even with slight change in pH.

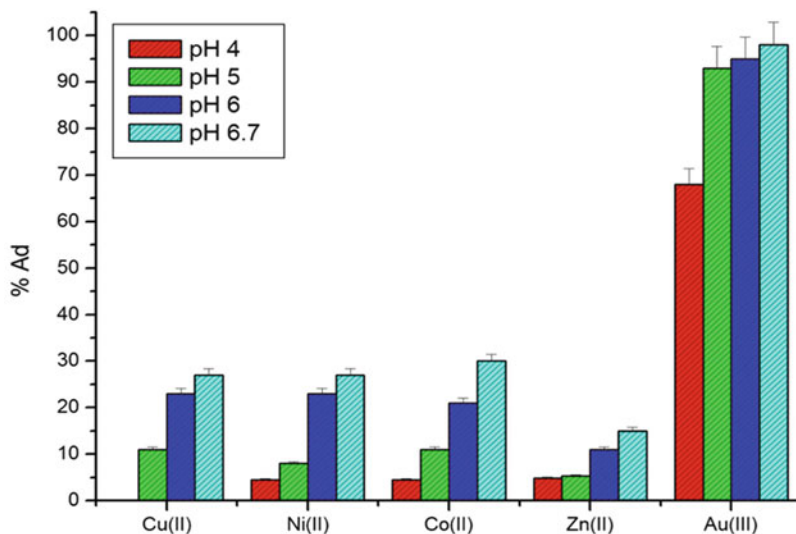


Fig. 11 pH-dependent adsorption for SMA beads (Gonte 2013)

Effect of SMA Copolymer Dose

An increase in the amount of adsorbents leads to a significant increase in the active sites which shows an enhanced adsorption of various metal ions and dyes. Thus, it was observed that adsorption increases with increase in SMA dose of 0.1 g–1.0 g (Fig. 12). However, further increase in sorbent dose showed no significant increase in adsorption. This can be attributed to the presence of very low concentration of metal ions/dyes in the solution such that the equilibrium is achieved, and no further adsorption occurs. Removal of metal ions increases with increased adsorbent dosage due to increase in active sites.

Equilibrium Adsorption Isotherms

The distribution of adsorbed chemical species between the liquid phase and the solid phase at equilibrium state was studied by fitting the obtained experimental equilibrium data to the various adsorption isotherm models, namely, Langmuir model, Freundlich model, Temkin model and Dubinin-Radushkevich (D-R) model. Adsorption isotherm graphs, i.e. equilibrium adsorption capacity (q_e) versus equilibrium concentration of the residual metal ions/dye in the solution (C_e), were plotted. The equilibrium adsorption capacity was calculated using the equation:

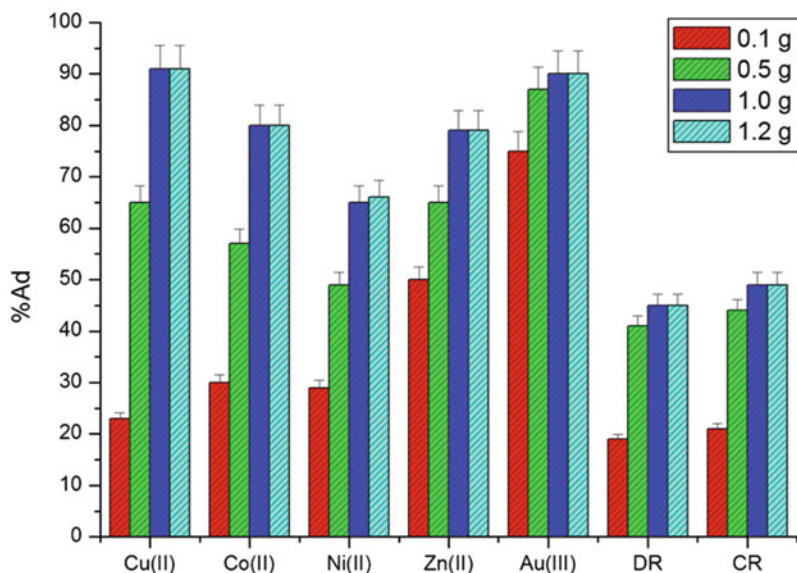


Fig. 12 Effect of SMA dose on adsorption of metal ions/dyes (Gonte 2013)

$$q_e = \frac{(C_0 - C_e)}{V} \times M$$

where q_e (mgg^{-1}) is the equilibrium adsorption capacity, C_0 and C_e are the initial and equilibrium concentration (mgL^{-1}) of metal ions/dye in solution, V (L) is the volume of solution and M (g) is the weight of the adsorbent used.

Langmuir Isotherm Model

Langmuir model postulates monomolecular layer adsorption without any interaction between the adsorbed molecules, and linearized form of this equation is represented as (Hostetler et al. 1998):

$$\frac{C_e}{q_e} = \frac{1}{q_{\max} \times K_L} + \frac{C_e}{q_{\max}}$$

where C_e is the equilibrium concentration (mgL^{-1}), q_e is the amount of metal ion sorbed (mgg^{-1}), q_{\max} is q_e for a consummate monolayer (mgg^{-1}) and K_L is a constant cognate to the affinity of the binding sites (Lmg^{-1}).

The plot of C_e/q_e versus C_e as shown in Fig. 13 yields the Langmuir constants q_{\max} and K_L . R_L is calculated from the initial conc. of metal ion/ dye as:

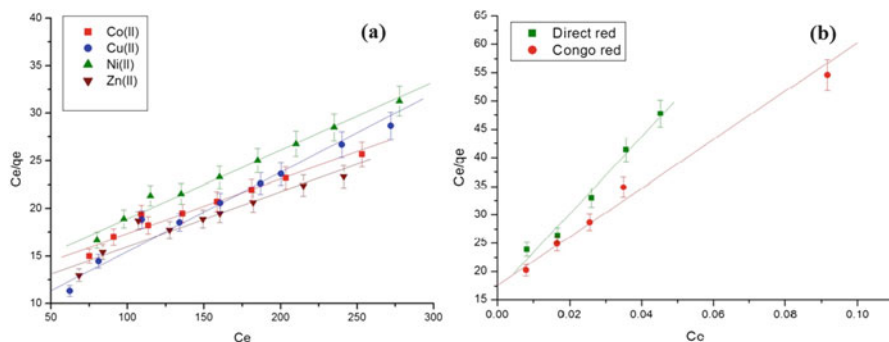


Fig. 13 Langmuir plots for adsorption of (a) metal ion (b) dyes (Gonte 2013)

$$R_L = \frac{1}{1 + (K_L \times C_0)}$$

The R_L value obtained for all the metal ions and dyes are greater than zero and less than unity indicating that the adsorption occurs as monolayer adsorption onto the heterogeneous/microporous surface of the SMA beads. The regression coefficient values of Cu (II), Co (II), Ni(II), Zn(II), Au(III), direct red and Congo red are 0.9755, 0.9798, 0.9896, 0.9548, 0.9813, 0.9905 and 0.9911, respectively. The high regression coefficient values of 0.97–0.99 indicate a high correlation between the experimental and theoretical data.

Freundlich Isotherm Model

The Freundlich isotherm model postulates adsorption occurs on heterogeneous surfaces and adsorption capacity is cognate to the concentration of metal ions at equilibrium. The linearized form of Freundlich equation is:

$$\ln q_e = \frac{1}{n} \times \ln C_e + \ln K_F$$

where q_e and C_e are the equilibrium concentrations of metal ions in adsorbed (mg/g) and liquid phases (mg/L), respectively. K_F and n are the Freundlich constants related to adsorption capacity and intensity, respectively.

The plot of $\ln q_e$ versus $\ln C_e$ is shown in Fig. 14 and yields the value of Freundlich constant n and K_F . A favourable adsorption is indicated from the values of the order Cu(II) > Au(III) > Ni (II) > Zn (II) > Co (II) > Congo red > direct red. The regression coefficient values of Cu (II), Co (II), Ni(II), Zn(II), Au(III), direct red and Congo red are 0.9939, 0.9792, 0.9972, 0.9994, 0.9988, 0.9919 and 0.9948, respectively. The regression coefficients (≈ 0.99) also indicate a high correlation of the experimental data with the theoretical calculations.

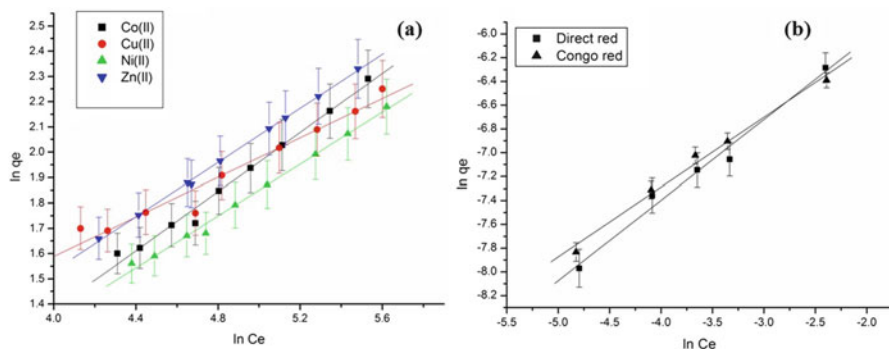


Fig. 14 Freundlich plots for adsorption of (a) metal ions and (b) dyes (Gonte 2013)

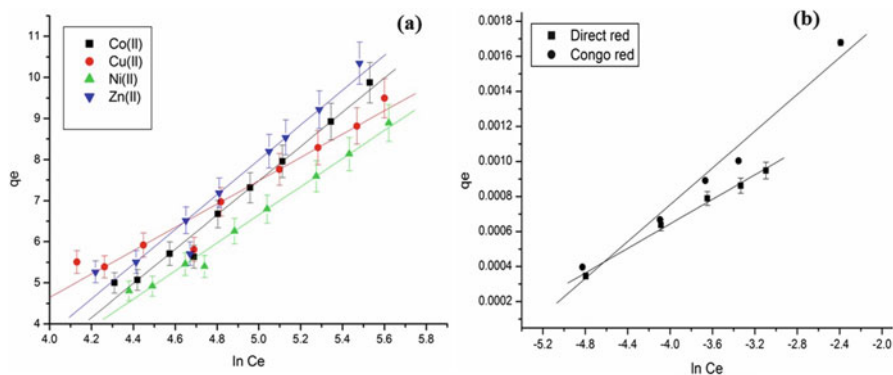


Fig. 15 Temkin plots for adsorption of (a) metal ions, (b) Au(III) ions and (c) dyes (Gonte 2013)

Temkin Isotherm Model

The effects of heat of adsorption that decrements linearly with coverage of the adsorbate and adsorbent interactions are postulated by the Temkin's model which is represented as:

$$q_e = \frac{RT}{bT} \times (\ln \alpha T) + \frac{RT}{bT} \times \ln C_e$$

where R is the gas constant $8.314 \times 10^{-3} \text{ kJ mol}^{-1} \text{ K}^{-1}$, T is the absolute temperature K , bT is the Temkin constant related to the heat of adsorption (kJ mol^{-1}) and αT is the equilibrium binding constant corresponding to the maximum binding energy (l/g).

The linear plots of q_e versus $\log C_e$ determines the constants αT and bT (Fig. 15). The regression coefficient values of Cu (II), Co (II), Ni(II), Zn(II), Au(III), direct red and Congo red are 0.9743, 0.9896, 0.9936, 0.9760, 0.9810, 0.9959 and 0.9875, respectively. The satisfactory linear fit obtained for all metal ions and dyes is indicated from the regression coefficient values.

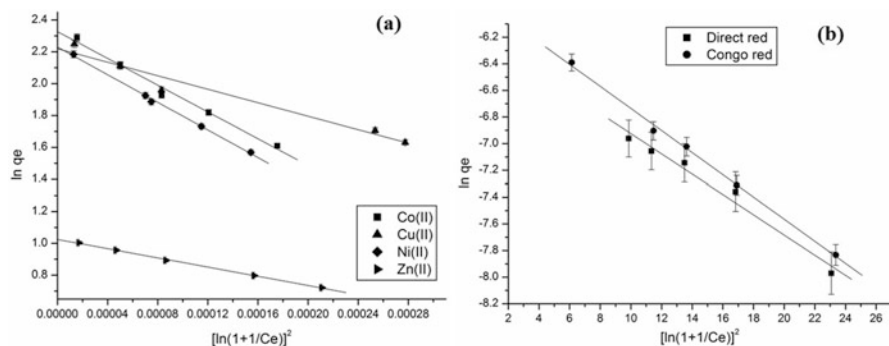


Fig. 16 Dubinin-Radushkevich plots for adsorption of (a) metal ions and (b) dyes (Gonte 2013)

Dubinin-Radushkevich (D-R) Isotherm Model

Dubinin-Radushkevich models estimate the mean free energy of adsorption. The linearized form of the D-R equation is represented as:

$$\ln q_e = \ln q_{\max} - K\epsilon^2$$

where K ($\text{mol}^2 \text{kJ}^{-2}$) is a constant related to the mean adsorption energy and ϵ is the Polanyi potential, calculated from equation:

$$\epsilon = RT \ln \left(1 + \frac{1}{C_e} \right)$$

The plot of $\ln q_e$ versus ϵ^2 (Fig. 16) yields the constant K , which presages the mean free energy E of adsorption per molecule of the adsorbate when it is transferred to the surface of the solid from illimitability in the solution. The regression coefficient values of Cu (II), Co (II), Ni(II), Zn(II), Au(III), direct red and Congo red are 0.9743, 0.9896, 0.9936, 0.9760, 0.9810, 0.9959 and 0.9875, respectively. The adsorption is assumed to be physisorption in the early stages followed by chemisorption of the chemical species involved.

Kinetic Studies

Kinetic experiments were conducted to determine the adsorption mechanism and the potential rate-controlling steps. These kinetic results also enable to select the optimum condition for full-scale batch adsorption process. The rate constants were calculated by using the conventional rate expression. The amount of metal ion/dye sorbed, q_t , was calculated as:

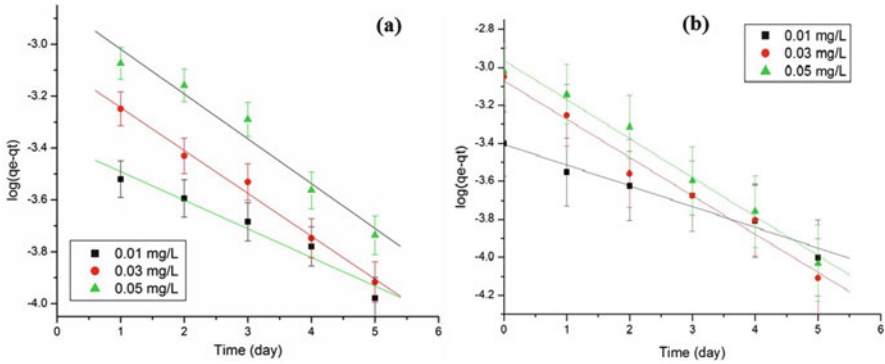


Fig. 17 Pseudo-first-order plots for adsorption of (a) direct red and (b) Congo red dye (Gonte 2013)

$$q_t = \frac{(C_o - C_t)}{M} \times V$$

where q_t (mg/g) is the equilibrium adsorption capacity.

Pseudo-First-Order Kinetic Model

This kinetic model assumes that rate of adsorption of solute on the adsorbent is based on the adsorption capacity. The pseudo-first-order rate equation is given as:

$$\log(q_e - q_t) = \log q_e - \frac{k_1}{2.303} \times t$$

where k_1 is the first-order adsorption rate constant (min^{-1}). The graph of $\log (q_e - q_t)$ versus t gives a straight line plot (Fig. 17) with negative slopes from which the pseudo-first-order rate constant is calculated. The correlation coefficient values of dyes (0.99) obtained by this method show good quality of linearization.

Pseudo-Second-Order Kinetic Model

The pseudo-second-order kinetic models correlate between the amount of metal ions/dye on the adsorbent surface and its amount adsorbed at equilibrium. The rate is directly proportional to the number of active surface sites, which is calculated as:

$$\frac{t}{q_t} = \frac{1}{k_2 \times q_e^2} + \frac{1}{q_e} \times t$$

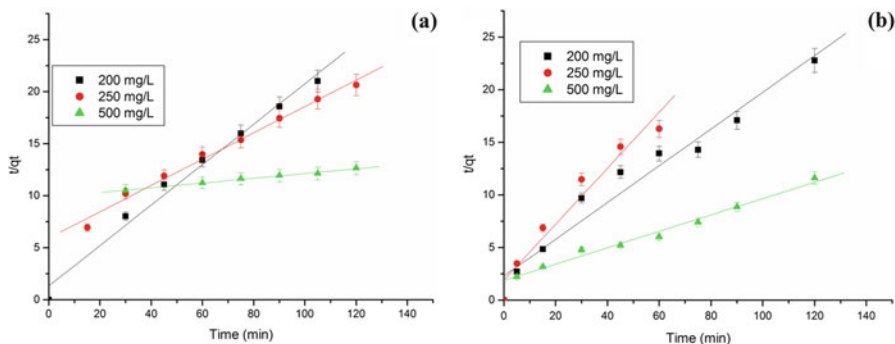


Fig. 18 Pseudo-second-order plots for adsorption of (a) Cu(II) and (b) Zn(II) ions (Gonte 2013)

where k_2 is the second-order adsorption rate constant ($\text{mg g}^{-1} \text{min}^{-1}$). The constant k_2 is used to calculate the initial sorption rate h ($\text{mg}/(\text{g min})$), at $t \rightarrow 0$ as follows:

$$h = k_2 \times q_e^2$$

The application of the pseudo-second-order kinetics by plotting t/q_t versus t (Fig. 18) yielded the second-order rate constant k_2 . The calculated q_e values for Cu(II) and Zn(II) agree very well with the experimental values as compared to other metal ions and dyes; however, the correlation coefficient obtained for all the adsorbates gives best fit linearized plots.

Adsorption Mechanism

The mechanism involved in the adsorption of metal ions and dyes onto the SMA beads was identified by fitting the experimental data to the intraparticle diffusion plot, a graph of q_t versus $t^{1/2}$ (Fig. 19) from the equation:

$$q_t = K_{\text{int}} \times t^{1/2}$$

where K_{int} is the intraparticle diffusion rate constant ($\text{mg g}^{-1} \text{min}^{-0.5}$).

The first sharper portion is the external surface adsorption, the second portion is the gradual adsorption stage and the third step is the final equilibrium stage. The three-step adsorption process was observed only for the metal ions, whereas for dyes only two-step adsorption was indicated without achieving the final equilibrium stage.

Desorption Studies

The reusability of the SMA beads was tested by observing the desorption of the various metal ions and dyes from the cross-linked SMA bead surface using hydrochloric acid solutions. Desorption ratio was calculated from the equation:

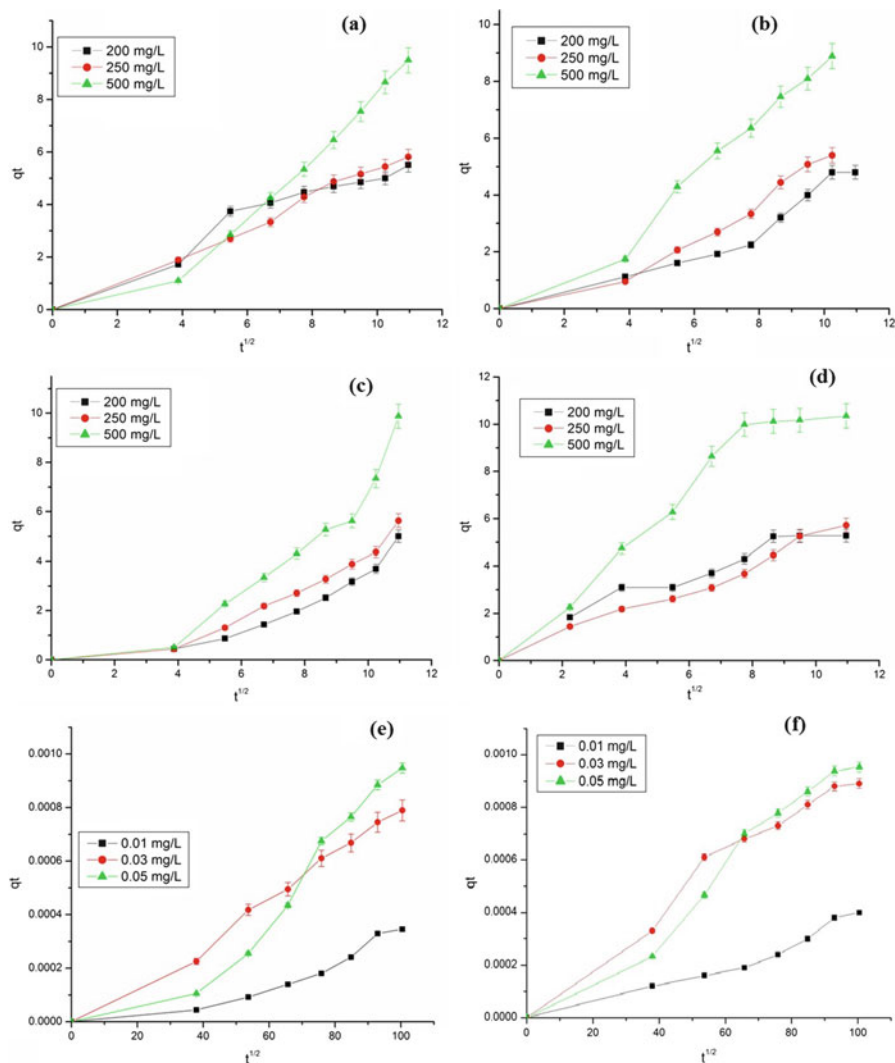


Fig. 19 Intraparticle diffusion graphs of (a) Cu(II), (b) Ni(II), (c) Co(II), (d) Zn(II), (e) direct red and (f) Congo red dye (Gonte 2013)

$$\text{Desorption ratio} = \frac{\text{amt.of adsorbate desorbed}}{\text{amt.of adsorbate adsorbed}} \times 100$$

Rapid desorption ($\approx 80\%$) of metal ions was noted within the first 10 min as can be observed from Fig. 20. It can be clearly noted that desorption of Cu (II) ions occurs to its maximum 97% within 15 min after which no further desorption occurred. Desorption of Ni(II) and Co(II) reached its maximum within 30 min. In case of dyes, $\approx 85\%$ complete desorption occurred using 0.5 M HCl solution in

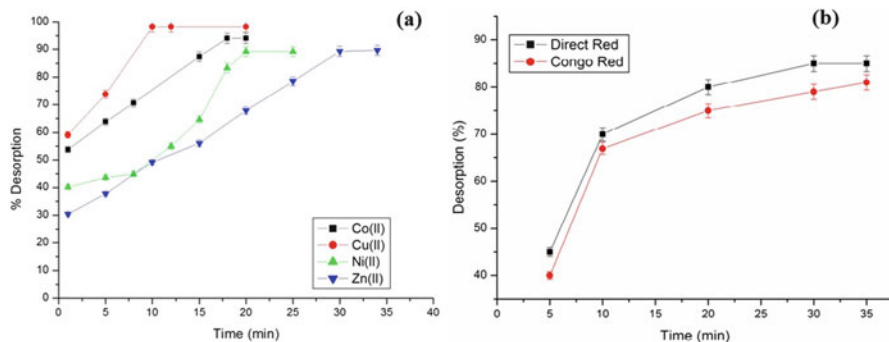


Fig. 20 Desorption curves of (a) metal ions and (b) dye (Gonte 2013)

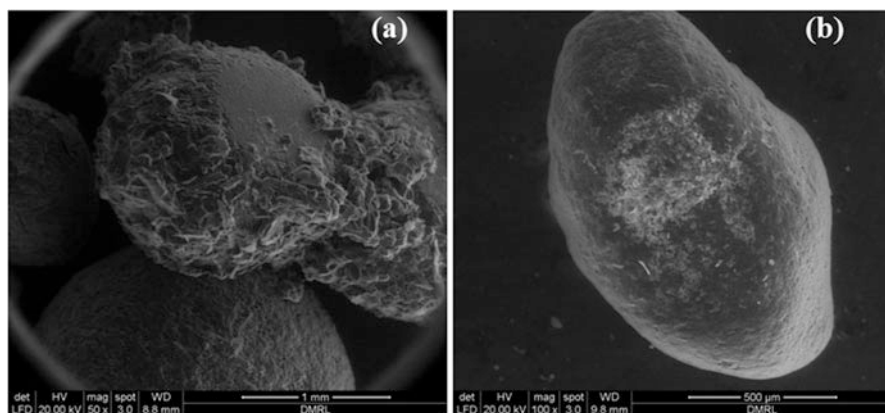


Fig. 21 SEM images of (a) SD-SMA and (b) SM-SMA (Gonte 2013)

30 min. Thus the results show that the cross-linked SMA copolymer beads can be successfully regenerated and can be used for re-adsorption of metal ions/dyes from aqueous solution.

SMA Biocomposites

The SD-SMA and SM-SMA composite beads with varying wt% of biomaterials (5 wt %, 10 wt% and 20 wt%) were synthesized. It was observed that uniform-sized spherical beads were developed with addition of sawdust up to 20 wt%, and with sugarcane molasses, elliptical beads of uniform size were obtained up to 10 wt% addition. Additionally, the SEM images of the composite beads (SD-SMA and SM-SMA) formed were in the size range 300–600 μm as can be seen from the SEM micrographs. The micrographs also confirmed the spherical shape of SD-SMA composite beads (Fig. 21a) and elliptical shape of SM-SMA composite beads (Fig. 21b).

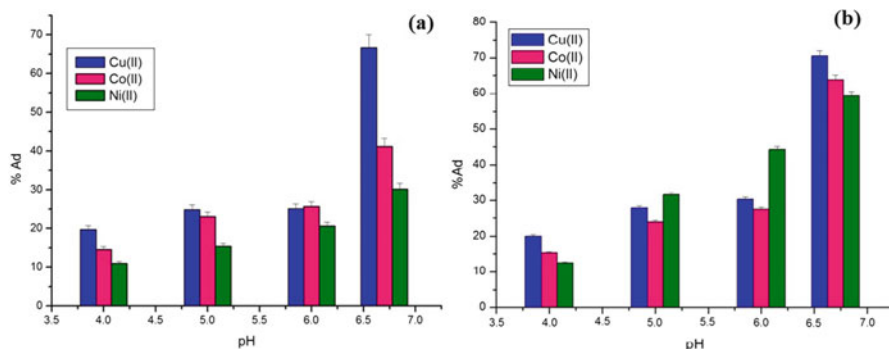


Fig. 22 Effect of pH on adsorption using (a) SD-SMA and (b) SM-SMA composite (Gonte 2013)

Effect of Solution pH

The adsorption of Congo red dye was studied at pH 7. The Congo red dye was found to be chemically and structurally stable at pH 7. Drastic colour change was described with remote transmutation in pH. The adsorption of metal ions (Cu(II), Co(II) and Ni(II)) was studied by varying the pH of the solution from pH 4.0 to pH 8. It was observed adsorption increases with increase in the pH of the solution, exhibiting maximum adsorption at pH 6.7 (Fig. 22). The SM-SMA composite beads demonstrated enhanced adsorption as compared to SD-SMA composite groups which can be attributed to the astronomically immense number of lignin and cellulosic groups of SM.

Effect of Composite Dose

Increasing the amount of composite beads from 0.1 to 0.5 g for a fixed volume of solution at pH 6.7 and 200 mgL^{-1} metal ion conc., adsorption was observed to increase which is due to significant increase in the active adsorption sites. The enhanced adsorption was again noted with SM-SMA composite beads (Fig. 23). However, further increase in sorbent dose showed no significant increase in adsorption.

Equilibrium Adsorption Isotherms

Langmuir Model

Langmuir model was found to be applicable in the interpretation of adsorption of CR dye and metal ions (Fig. 24) onto SD-SMA and SM-SMA composite beads. The equilibrium data when validated with the theoretical equation (Sousa et al. 2009)

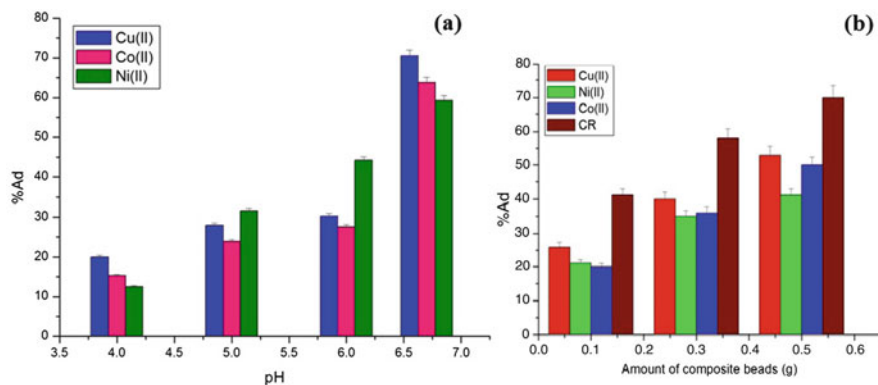


Fig. 23 Effect of composite dose on adsorption of metal ions and dye using (a) SD-SMA and (b) SM-SMA (Gonte 2013)

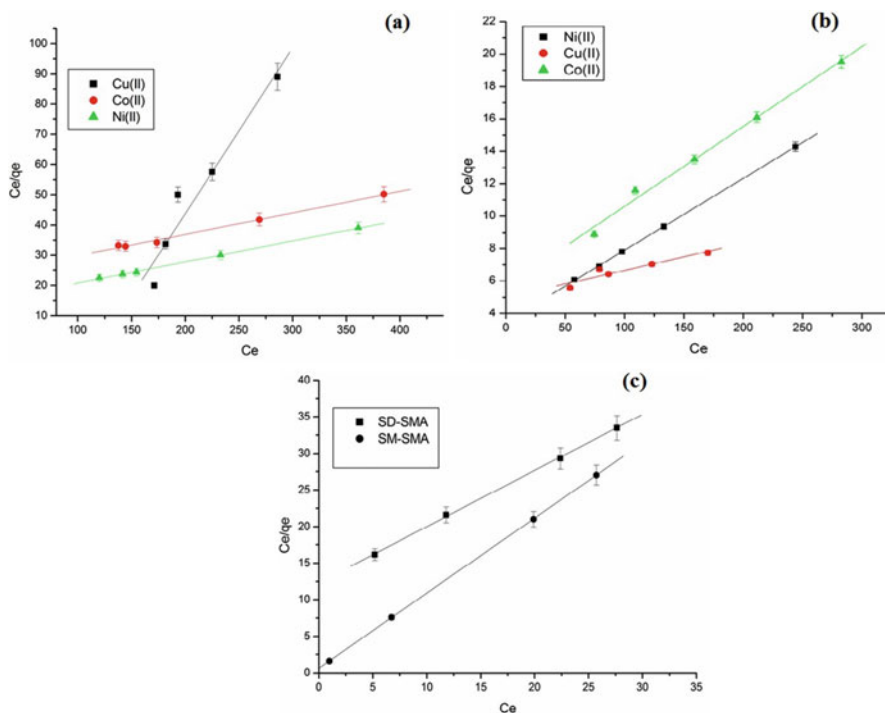


Fig. 24 Langmuir adsorption isotherm for adsorption of metal ions onto (a) SD-SMA and (b) SM-SMA and adsorption isotherm for (c) CR (Gonte 2013)

gave rise to the linear plots, indicating that the Langmuir model could be well applied to the system:

$$\frac{C_e}{q_e} = \frac{1}{q_{\max} \times K_L} + \frac{C_e}{q_{\max}}$$

Freundlich Model

The Freundlich constants were calculated by plotting graph of $\ln q_e$ versus $\ln C_e$ using the linearized isotherm equation (Zuorro et al. 2010; Zhang et al. 2010) for adsorption of dyes and metal ions (Fig. 25) onto the biocomposite beads:

$$\ln q_e = \frac{1}{n} \times \ln C_e + \ln K_F$$

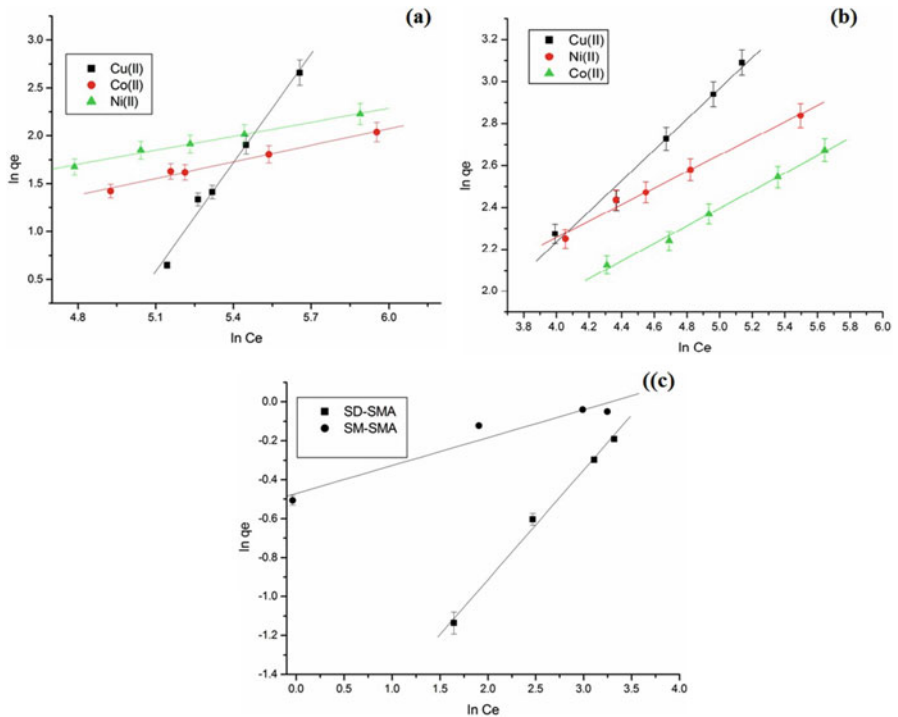


Fig. 25 Freundlich adsorption isotherm for adsorption of metal ions onto (a) SD-SMA and (b) SM-SMA and adsorption isotherm for (c) CR (Gonte 2013)

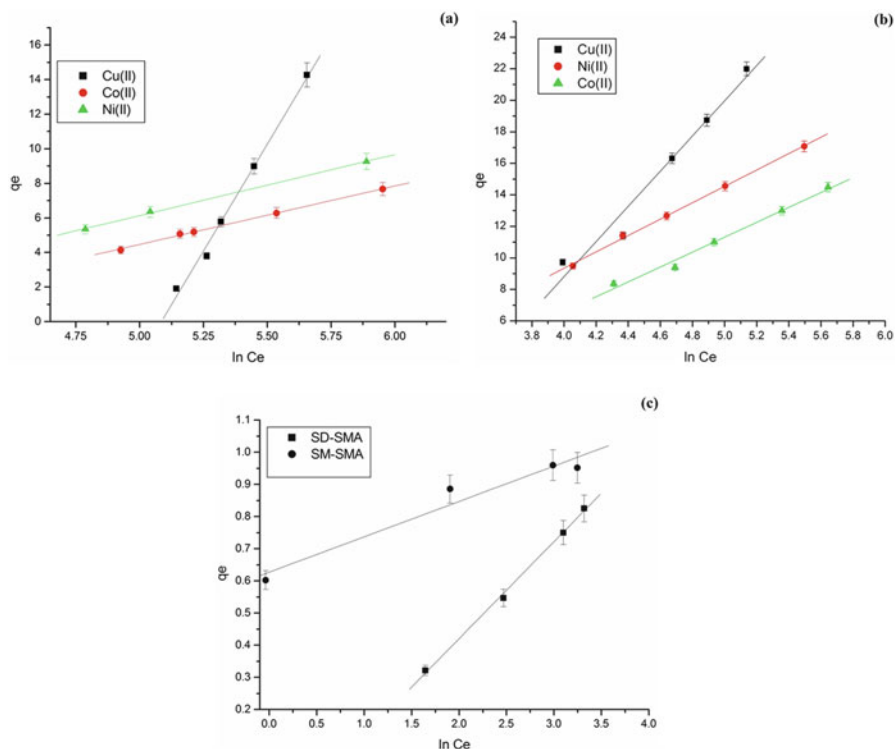


Fig. 26 Temkin adsorption isotherm for adsorption of metal ions onto (a) SD-SMA and (b) SM-SMA and adsorption isotherm for (c) CR (Gonte 2013)

Temkin Model

Temkin isotherm model was used to calculate the maximum binding energy using the linearized equation (Zuorro and Lavecchia 2010) as:

$$q_e = \frac{RT}{bT} \times (\ln \alpha T) + \frac{RT}{bT} \times \ln C_e$$

The graph of q_e versus $\ln C_e$ for adsorption of dyes and metal ions (Fig. 26) yields the value of αT corresponding to the maximum binding energy. The values indicate a good potential for adsorption of metal ions and dyes onto the composite beads with high correlation coefficient values.

Kinetic Models

Pseudo-First-Order

Lagergren pseudo-first-order linearized equation was used to determine the adsorption mechanism (Demirbas et al. 2002):

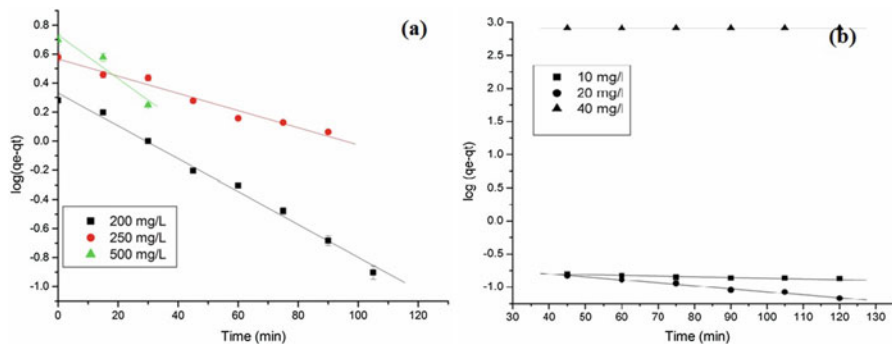


Fig. 27 Pseudo-first-order plots using SD-SMA for adsorption of (a) Cu(II) and (b) CR (Gontе 2013)

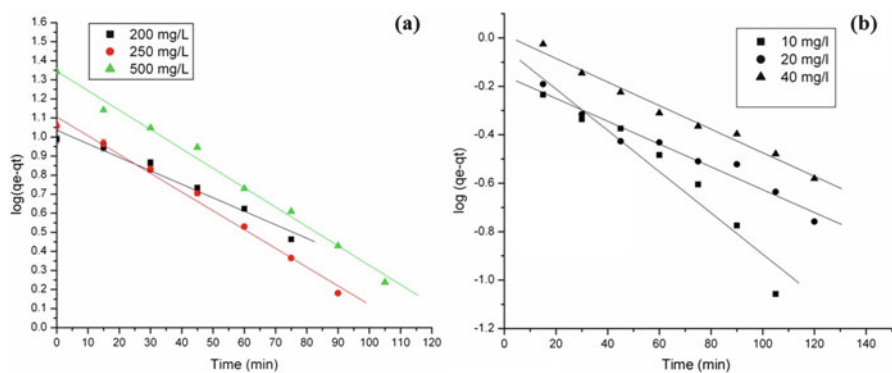


Fig. 28 Pseudo-first-order plots using SM-SMA for adsorption of (a) Cu(II) and (b) CR (Gontе 2013)

$$\log(q_e - q_t) = \log q_e - \frac{k_1}{2.303} \times t$$

The linearized graphs of the pseudo-first-order kinetics of Cu(II) and CR are presented in Figs. 27 and 28 for SD-SMA and SM-SMA composite beads, respectively. The rate constants obtained for all the different conc. of metal ions are also comparable indicating the same adsorption mechanism applies and that adsorption occurs by monolayer formation onto the composite beads, thus suggesting that a pseudo-first-order rate governs the adsorption process.

Pseudo-Second Order

The linearized pseudo-second-order rate equation (Demirbas et al. 2002) was used to calculate the rate constant in predicting the rate control kinetics:

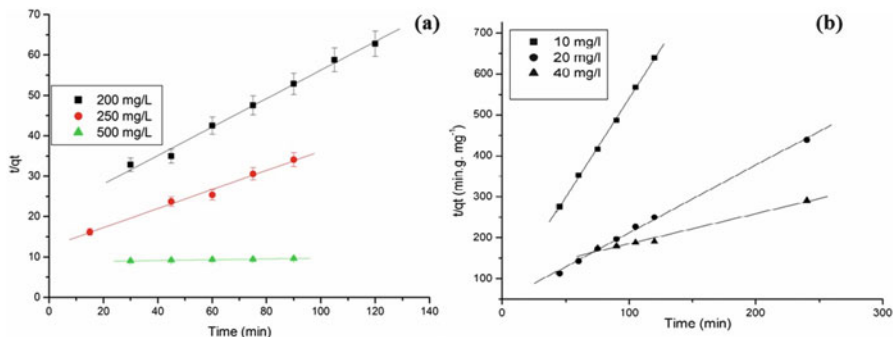


Fig. 29 Pseudo-second-order plots using SD-SMA for adsorption of (a) Cu(II) and (b) CR (Gonte 2013)

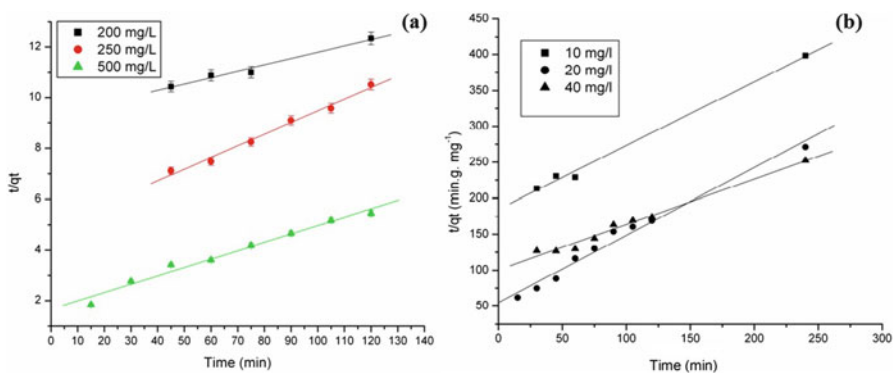


Fig. 30 Pseudo-second-order plots using SM-SMA for adsorption of (a) Cu(II) and (b) CR (Gonte 2013)

$$\frac{t}{q_t} = \frac{1}{k_2 \times q_e^2} + \frac{1}{q_e} \times t$$

The linearized form of the pseudo-second-order model for SD-SMA and SM-SMA composite beads for Cu(II) and CR is shown in Figs. 29 and 30, respectively. The high correlation coefficient values obtained for metal ions and dyes support the assumption that adsorption of metal ions is through chemisorption involving valence forces through the sharing or exchange of electrons between adsorbent and metal ions.

Intraparticle Diffusion Model

Intraparticle diffusion model was used to describe the adsorption mechanism onto SD-SMA and SM-SMA composite beads. Figures 31 and 32 show the plot

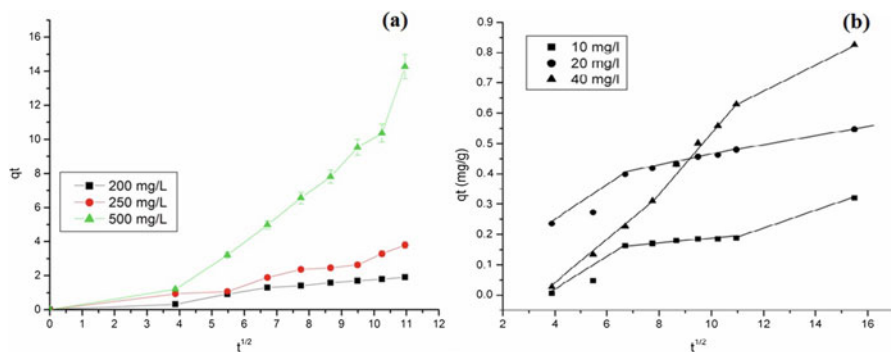


Fig. 31 Intraparticle diffusion plots using SD-SMA for adsorption of (a) Cu(II) and (b) CR (Gonte 2013)

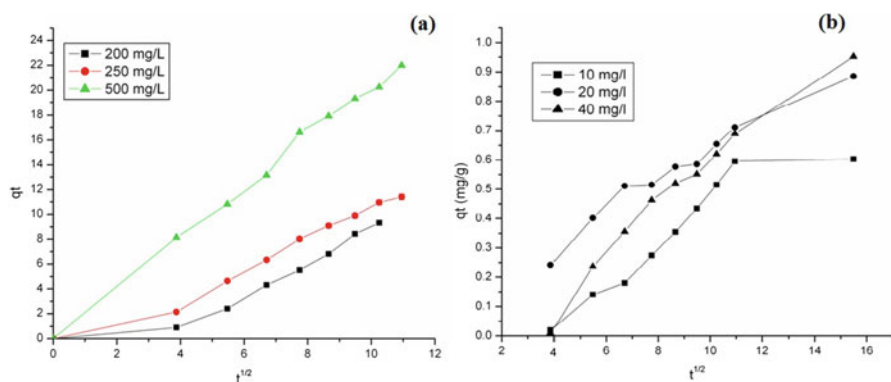


Fig. 32 Intraparticle diffusion plots using SM-SMA for adsorption of (a) Cu(II) and (b) CR (Gonte 2013)

of q_t vs $t^{1/2}$ for Cu(II) and CR on SD-SMA and SM-SMA composite beads. Adsorption occurs in two-step adsorption. The first is the instantaneous diffusion, where the rate of diffusion is fast, and the second step is a rate-controlled step. These observations are in good agreement with the literature (Parab et al. 2010).

Chemically Modified SMA Beads

Characterization

The FTIR spectra of SMA-MOFs beads showed a drastic decrease carboxylate ion 1725 cm^{-1} peak indicating the formation of metal carboxylates into the polymer matrix as can be clearly seen from Fig. 33a. The presence of 1311 cm^{-1} peak

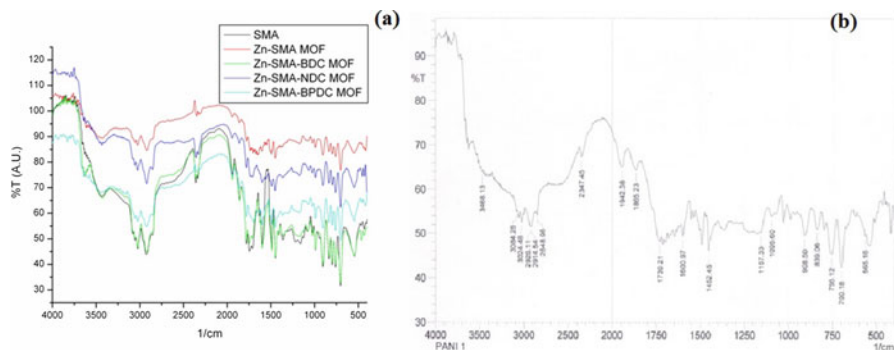


Fig. 33 Hydrogen adsorption onto SMA beads (Gonte 2013)

corresponding to aromatic C-N stretch, the asymmetric stretching frequency of N-H at 3335 cm^{-1} , C-N stretch at 1172 cm^{-1} and a low-intensity 1620 cm^{-1} (sharp peak) corresponding to N-H bends were observed in FTIR spectrum of SMA-PANI IPNs (Fig. 33b). Thus the presence of C-N and N-H peaks in the IR spectrum indicates the formation of polyaniline in the semi-IPN. Moreover, the CHNS-elemental analysis of PANI-encapsulated SMA polymer showed the presence of 0.395% N corresponding to $\approx 2:8$ mole% of polyaniline in the semi-IPNs. The SEM analysis of the cut surface of the modified SMA beads revealed well-defined structure formation in the interiors/pores of the SMA beads. The thermal stability of the various modified polymer matrixes were confirmed from the thermogravimetric analysis (TGA), which revealed no change in the shape of the decomposition curve on formation of metal complexes or semi-IPNs as compared to the SMA copolymer. The chemical modifications showed no effect on the thermal stability of the polymer matrix, exhibiting the usable temperature range from RT to $400\text{ }^{\circ}\text{C}$. The residual mass, however, decreased by 7–10%, which is expected due to the formation of metal-carboxylate complexes with the carboxylic acid groups which decrease the concentration of maleic anhydride content of the polymer.

Hydrogen Adsorption

The hydrogen adsorption studies were conducted by allowing the beads to be in contact with the gas in discreet pressure ranges within 0–900 torr. For this study, a Sorptomatic 1900, which allows accurate measurements up to 900 torr, has been used (Gonte et al. 2012). All the measurements were carried out at room temperature 300 K.

It was observed that the rate of hydrogen adsorption is almost comparable for the various cross-linked polymers, independent of their DVB content (Fig. 34).

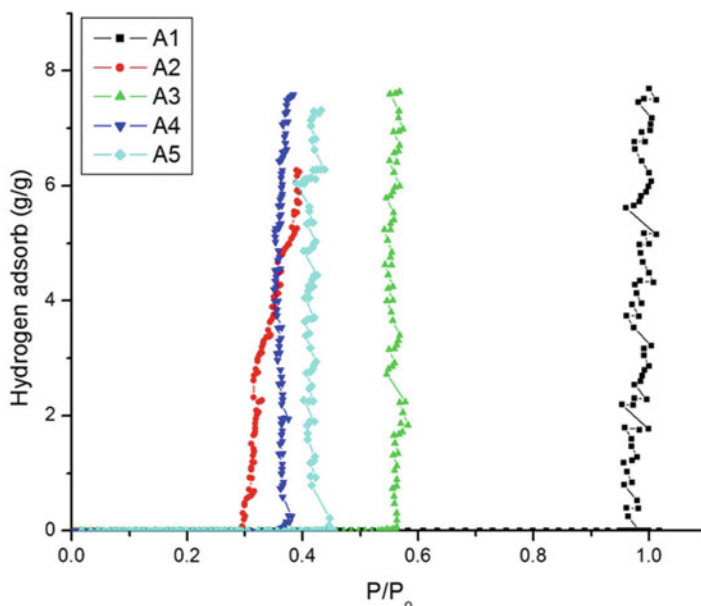


Fig. 34 Hydrogen adsorption onto modified SMA beads (Gonte 2013)

Hydrogen adsorption analysis on SMA beads under the same desired acquisition parameters as observed by (Deb et al. 2005) showed the rate of adsorption to be 3 wt% per hr., as compared to the highly cross-linked beads where the rate is about 30 wt% per h. In the case of A1, A3 and A5, positive adsorption was observed. These results are in good agreement with the previously reported results on hydrogen adsorption in the SMA copolymer matrix (Deb et al. 2005).

Hydrogen adsorption in the Zn-SMA-MOF beads and Zn-SMA-DCA MOFs beads were also studied under the same parameters at room temperatures (300 K) (Fig. 35). Instantaneous hydrogen adsorption on these beads for 25 h revealed that hydrogen storage capacity of the hypercross-linked polymer beads (0.67 wt %) decreases slightly due to the formation of metal complex and entrapment of MOFs in the pores. These findings can be attributed to the blockage of pores by the complex formation and MOF decoration. This effect was found to diminish with long exposure time of 3 days where similar hydrogen adsorption capacity (≈ 0.8 wt%) was noted for all types of beads (Gonte et al. 2011a, b).

With PANI-encapsulated polymer, the adsorption was observed to take place at around 500 torr pressure and showed continuous uptake without reaching the limiting saturation pressure. The decrease in the rate of hydrogen adsorption by PANI-encapsulated polymers indicates towards the decrease in the pore size due encapsulation, which occurs even in the pores of the SMA polymer microspheres. The size of the pore and overall microsphere diameter has found to have a profound influence on the hydrogen adsorption capacity of the polymer. However, the pore surface of the SMA polymer that is coated with polyaniline will tend to reduce the

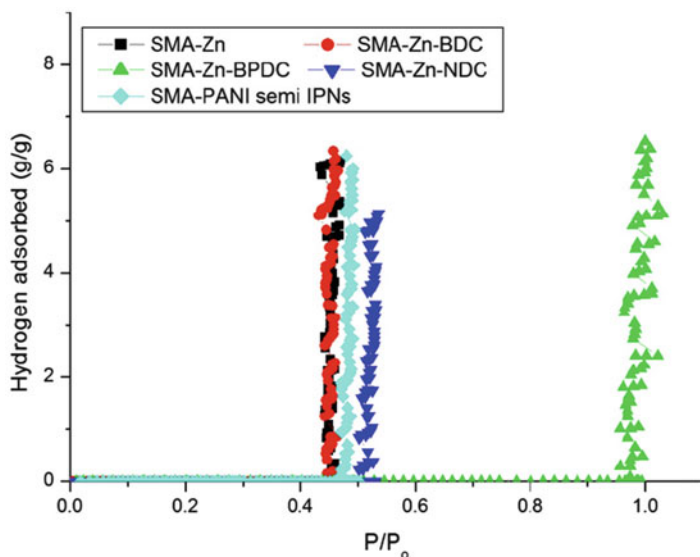


Fig. 35 Hydrogen adsorption onto modified SMA beads (Gonte 2013)

porosity of the polymer as confirmed from SEM findings (Gonte et al. 2011a, b) which results in decrease in hydrogen adsorption capacity.

Conclusions

The present chapter describes about the styrene-maleic acid copolymer beads as adsorbent for removal of heavy metal ions and dyes from aqueous solutions and also as adsorbent material for hydrogen storage. Thus the copolymer matrix was synthesized by suspension polymerization method which yields the spherical bead-shaped copolymer. Effect of agitation speed on bead dimension was studied. Five different compositions were made varying the cross-linker divinylbenzene content, and the mechanical, morphological and thermal properties were analyzed and one final composition was selected as adsorbent. Characterization of SMA beads was carried out using various techniques such as FTIR, SEM, TGA, XRD and SAXS, and the effect of experimental parameters on adsorption were studied. Adsorption studies on cross-linked SMA beads were carried out using various adsorption isotherms and kinetic models. The results thus indicate that cross-linked SMA copolymer bead can prove to be a potential candidate for treatment of industrial wastewater containing various metal ions and dyes. These copolymer beads were also capable of in situ reduction of Au (III) to Au(0) without the use of any additional reducing or capping agents.

SMA-biocomposite beads were synthesized for the increment in the effectiveness of the adsorption process, and characterization studies were carried out. Biocomposites of SMA prove to be highly effective for the removal of dye stuffs supported by the obtained data. Langmuir, Freundlich and Temkin isotherm adsorption models were utilized for the mathematical analysis of the adsorption equilibrium for both SD-/SM-SMA composite beads. The results obtained by the adsorption isotherms gave best fit for experimental data, and the equilibrium could be well described by Langmuir and Freundlich isotherm models indicating monolayer adsorption in the first step followed by heterogeneous surface binding, suggesting chemisorptive uptake of metal ions and dye from aqueous solution. Hydrogen adsorption studies were carried out for both cross-linked SMA beads and chemically modified SMA beads. Enhanced rate of hydrogen adsorption at room temperature was successfully achieved by the introduction of highly cross-linked interpenetrating networks inside the microspheres. No drastic change in the rate of adsorption was noticed after complexation with Zn(II) suggesting the involvement of metal complexes in adsorption.

In summary, it is concluded that the cross-linked styrene-maleic acid copolymer beads can be considered as suitable adsorbent for removal of heavy metal ions and dyes having a wide concentration range in aqueous systems. Such copolymer matrix is highly effective for batch as well as for continuous flow process. These adsorbents can be effectively recycled for further use. Biocomposites of SMA prove to be highly effective for the removal of dye stuffs. Such cost-effective adsorbent using inexpensive removal technique can find wide industrial applications. Hydrogen adsorption can be achieved under optimized conditions.

References

- Abdel-Ghani N, Hegazy AK, El-Chaghaby G (2009) *Typha domingensis* Leaf powder for decontamination of aluminium, iron, zinc and lead: biosorption kinetics and equilibrium modelling. *Intl J Environ Sci Technol* 6:243–248
- Al-Asheh S, Banat FA, Abu-Aitah L (2003) Adsorption of phenol using different types of activated bentonites. *Sep Purif Technol* 33:1–10
- Al-Rekabi WS, Qiang H, Qiang WW (2007) Improvements in wastewater treatment technology. *Pak J Nutr* 6:104–110
- Atia A, Donia AM, Abou-El-Enein SA (2003) Studies on uptake behavior of copper(II) and lead (II) by amine chelating resins with different textural properties. *Separat Purif Technol* 33:295–301
- Azanova VV, Hradil J (1999) Sorption properties of macroporous and hyper-crosslinked copolymers. *React Func Polym* 41:163–175
- Babel S, Opiso EM (2007) Removal of Cr from synthetic wastewater by sorption into volcanic ash soil. *Intl J Environ Sci Technol* 4:99–108
- Celik A, Demirbas A (2005) Removal of heavy metal ions from aqueous solutions via adsorption onto modified lignin from pulping wastes. *Energy Sources* 27:1167–1177
- Corapcioglu M, Huang C (1987) The adsorption of heavy metals onto hydrous activated carbon. *Water Res* 21:1031–1044

- Davankov V, Tsyurupa M (1990) Structure and properties of hyper crosslinked polystyrene – the first representative of a new class of polymer networks. *React Polym* 13:27–42
- Deb PC, Mathew A (1996) Synthesis of spherical copolymer beads of styrene-maleic anhydride by aqueous suspension polymerization. *J Polym Sci Part A Polym Chem* 34:1605–1607
- Deb PC, Rajput LD, Agrawal AK, Singh PK, Hande V, Sasane S (2005) Crosslinked styrene-maleic acid copolymer complexes of some transition metals and their adsorption behaviour. *Polym Adv Technol* 16:681–687
- Demirbas O, Alkan M, Sousa MW, Sousa M, Oliveira IR, Oliveira A, Cavalcante R, Fachine P et al (2002) The removal of Victoria blue from aqueous solution by adsorption on a low-cost material. *Adsorption* 8:341–349
- Den S (2006) Sorbent technology – encyclopedia of chemical processing; CRC Press, Taylor & Francis Group
- Deng S, Ting YP (2005) Polyethylenimine-modified fungal biomass as a high capacity adsorbent for chromium anion removal. *Environ Sci Technol* 39:8490–8496
- Deshdmukh JH, Deshpande MN (2011) X-ray diffraction studies of Cu (II), Co (II), Fe (II) complexes with (RS)-4-(7-chloro-4-quinolyl amino) pentyldiethylamine diphosphate. *J Chem Pharmaceut Res* 3:706–712
- Donmez C, Aksu Z, Ozturk A, Kutsal T (1999) A comparative study on heavy metal biosorption characteristics of some algae. *Process Biochem* 34:885–892
- Farajzadeh MA, Fallahi MR (2005) Study of phenolic compounds removal from aqueous solution by polymeric sorbent. *J Chinese Chem Soc* 52:295–301
- Febrianto J, Kosasih A, Sunarso J, Ju Y, Indraswati N, Ismadji S (2009) Equilibrium and kinetic studies in adsorption of heavy metals using biosorbent: a summary of recent studies. *J Hazard Mater* 162:616–645
- Goltz HR, Jones KC, Tegen MH (1994) High surface area polymeric adsorbents for VOC capture and on-site regeneration. Air and Waste Management Association, 87th Annual Meeting and Exhibition, Cincinnati
- Gonte RR (2013) Styrene-maleic acid co-Polymer beads and composites for adsorption of toxic chemicals and hydrogen Dept Appl Chem Defence Inst Adv Technol (DU) – PhD Thesis.
- Gonte RR, Balasubramanian K, Deb P (2011a) Synthesis and characterization of metal organic frameworks. *Proc Intl Conf Nano Eng Adv Comput (ICNEAC-2011)* 1:529–531
- Gonte RR, Balasubramanian K, Deb P (2011b) Adsorption properties of crosslinked mesoporous (styrene – maleic acid) – Zn (II) complexes. *Intl J Indus Engg Technol* 3:279–288
- Gonte RR, Balasubramanian K, Deb PC, Singh P (2012) Synthesis and characterization of mesoporous hypercrosslinked poly (styrene Co-maleic anhydride) microspheres. *Intl J Polymeric Mater* 61:919–930
- Greig JA, Sherrington DC (2003) Molecular sieve behaviour in polymeric reagents. *Polymer* 19:163–172
- Gundogan R, Acemioglu B, Alma M (2004) Copper (II) adsorption from aqueous solution by herbaceous peat. *J Colloidal Interface Sci* 269:303–320
- Gupta V, Suhas (2009) Application of low-cost adsorbents for dye removal: a review. *J Environ Manag* 90:2313–2342
- Har MP, Fuller G, Brow AR, Dale JA, Plant S (2001) Sulphonated poly(styrene-co-divinylbenzene) ion exchange resins: acidities and catalytic activities in aqueous reactions. *J Mol Catalysis A Chem* 182-183:439–445
- Hostetler MJ, Wingate JE, Zhong CJ, Harris JE, Vachet RW, Clark MR et al (1998) Alkanethiolate gold cluster molecules with core diameter from 1.5 to 5.2 nm: Core and monolayer properties as a function of core size. *Langmuir* 14:17–30
- Inglezakis VJ, Loizidou MD, Grigoropoulou HP (2003) Ion exchange of Pb₂C, Cu₂C, and Cr₃C on natural clinoptilolite: selectivity determination and influence of acidity on metal uptake. *J Colloid Interface Sci* 261:49–54
- Issabayeva G, Aroua M, Sulaiman N (2007) Continuous adsorption of lead ions in a column packed with palm shell activated carbon. *J Hazard Mater* 155:109–113

- Jaber M, Miehé-Brendlé J, Michelin L, Delmotte L (2005) Heavy metal retention by organoclays: synthesis, applications, and retention mechanism. *Chem Mater* 17:5275–5281
- Kadirvelu K, Thamaraiselvi K, Namasivayam C (2001) Removal of heavy metals from industrial wastewaters by adsorption onto activated carbon prepared from an agricultural solid waste. *Bioresource Technol* 76:63–65
- Kapoor A, Viraraghavan T, Cullimore DR (1999) Removal of heavy metals using the fungus *Aspergillus niger*. *Bioresource Technol* 1:95–104
- Krysztafkiewicz A, Binkowski S, Jesionowski T (2002) Adsorption of dyes on a silica surface. *Appl Surf Sci* 199:3–39
- Lee JY, Wood CD, Bradshaw D, Rosseinsky M, Cooper A (2006) Hydrogen adsorption in microporous hypercrosslinked polymers. *Chem Commun* 25:2670–2672
- Leng Y (2009) *Materials characterization: introduction to microscopic and spectroscopic methods*. J. Wiley, Weinheim. ISBN: 978-3-527-33463-6
- Li H, Eddaoudi M, Groy TL, Yaghi OM (1998) Establishing microporosity in open metal-organic frameworks: gas sorption isotherms for Zn(BDC) (BDC=1,4- benzenedicarboxylate). *J Am Chem Soc* 120:8571–8572
- Markovska L, Meshko V, Marinkovski M (2006) Modeling of adsorption kinetics of zinc onto granular activated carbon and natural zeolite. *J Serbian Chem Soc* 71:957–967
- Netpradit S, Thiravetyan P, Towprayoon S (2004) Application of waste metal hydroxide sludge for adsorption of azo reactive dyes. *Water Res* 38:71–78
- Nwuche CO, Ugoji E (2008) Effects of heavy metal pollution on the soil microbial activity. *Intl J Environ Sci Technol* 5:409–414
- Odian G (2004) *Principles of polymerization*, 4th edn. J. Wiley, New Delhi. ISBN: 0-471-27400-3
- Omer Y, Yalcin A, Fuat G (2003) Removal of copper, nickel, cobalt and manganese from aqueous solution by kaolinite. *Water Res* 37:948–952
- Pan BC, Xiong Y, Su Q, Li AM, Chen JL (2003) Role of amination of a polymeric adsorbent on phenol adsorption from aqueous solution. *Chemosphere* 51:953–962
- Parab H, Joshi S, Sudersanan M, Shenoy N, Lali A, Sarma U (2010) Removal and recovery of cobalt from aqueous solutions by adsorption using low cost lingo cellulosic biomasscoir pith. *J Environ Sci Health Part A* 45:603–611
- Rawat J, Ahmad A, Agrawal A (1990) Equilibrium studies for the sorption of Cu^{2+} on lanthanum diethanolamine chelating material. *Colloid Surf* 46:239–253
- Rengaraj S, Kim Y, Joo C, Choi K, Yi J (2004) Batch adsorptive removal of copper ions in aqueous solutions by ion exchange resins: 1200H and IRN97H. *Korean Jo Chem Engg* 21:187–194
- Rengaraj S, Yeon J, Kimb Y, Jung Y, Ha Y, Kima W (2007) Adsorption characteristics of Cu (II) onto ion exchange resins 252H and 1500H: kinetics, isotherms and error analysis. *J Hazard Mater* 143:469–477
- Resmi G, Thampi S, Chandrakaran S (2010) *Brevundimonas vesicularis* : a novel bio-sorbent for removal of lead from wastewater. *Intl J Environ Res* 4:281–288
- Rivera-Utrilla J, Bautista-Toledo I, Ferro-Garcia MA, Moreno-Castilla C (2003) Bioadsorption of Pb(II) Cd(II), and Cr(VI) on activated carbon from aqueous solutions. *Carbon* 41:323–330
- Robinson T, Chandran B (2002) Studies on desorption of individual textile dyes and a synthetic dye effluent from dye adsorbed agricultural residues using solvents. *Bioresource Technol* 84:299–301
- Rosenberg G, Shabaeva A, Moryakov V, Musin T, Tsyurupa M, Davankov V (1983) Sorption properties of hypercrosslinked polystyrene sorbents. *React Polym Ion Exch Sorbents* 1:175–182
- Schlapbach L (2002) Hydrogen as a fuel and its storage for mobility and transport. *MRS Bull* 27:675–676
- Schlapbach L, Zuttel A (2001) Hydrogen storage materials for mobile application. *Nature* 414:353–358
- Shelar G, Gonte R, Ayalew AKB (2011) Porous biocomposite beads of sawdust for effluent treatment. *Proc Intl Conf Nano Eng Adv Comput (ICNEAC-2011)* 1:451–454

- Sicilia-Zafrac A, Gonzalez-Perez J, Niclos-Gutierrez J (1999) Synthesis, XRD structures and properties of Diaqua(iminodiacetato)copper(II), [Cu(IDA)(H₂O)₂], and 2,2-aqua(benzimidazole)(iminodiacetato)copper(II), [Cu(IDA)(hbzim)(H₂O)₂]. *Polyhedron* 18:3341–3351
- Sousa FW, Sousa M, Oliveira IR, Oliveira AG, Cavalcante RM, Fachine P et al (2009) Evaluation of a low-cost adsorbent for removal of toxic metal ions from wastewater of an electroplating factory. *J Environ Manag* 90:3340–3344
- Sternberg SPK, Dorn R (2002) Cadmium removal using cladophora in batch, semi-batch and flow reactors. *Bioresource Technol* 81:249–255
- Thomas WJ, Crittenden BD (1998) Adsorption technology and design. Butterworth-Heinemann, London
- Toro CA, Rodrigo R, Cuellar J (2009) Kinetics of the sulphonation of macroporous poly(styrene-co-divinylbenzene) microparticles. *Chem Engg Transc* 17:49–54
- Vasudevan P, Padmavathy V, Dhingra SC (2003) Kinetics of biosorption of cadmium on bakers yeast. *Bioresource Technol* 89:81–87
- Wan Y, Huang W, Wang Z, Zhu XX (2004) Preparation and characterization of high loading porous crosslinked poly(vinyl alcohol) resins. *Polymer* 45:71–77
- Wingenfelder U, Hansen C, Furrer G, Schulin R (2009) Removal of heavy metals from mine waters by natural zeolites. *Environ Sci Technol* 39:4606–4613
- Yang R (2003) Adsorbents: fundamentals and applications. Wiley, Hoboken
- Yavuz O, Altunkaynak Y, Guzel F (2003) Removal of copper, nickel, cobalt and manganese from aqueous solution by kaolinite. *Water Res* 37:948–952
- Zhang A, Asakura T, Uchiyama G (2003) The adsorption mechanism of uranium(VI) from seawater on a macroporous fibrous polymeric adsorbent containing amidoxime chelating functional group. *React Func Polym* 57:67–76
- Zhang Y, Li Y, Li X, Yang L, Bai X, Ye Z, Zhou L, Wang L (2010) Selective removal for Pb²⁺ in aqueous environment by using novel macroreticular PVA beads. *J Hazard Mater* 181:898–907
- Zhu J, Deng B, Yang J, Gang D (2009) Modifying activated carbon with hybrid ligands for enhancing aqueous mercury removal. *Carbon* 47:2014–2025
- Zuorro A, Lavecchia R (2010) Adsorption of Pb(II) on spent leaves of green and black tea. *Am J Appl Sci* 7:153–159